ABSTRACT

Title of thesis: A MODEL FOR NON-OXIDATIVE AND OXIDATIVE PYROLYSIS OF CORRUGATED CARDBOARD

Mollie Semmes, Master of Science, 2013

Directed by: Professor Stanislav I. Stoliarov
Department of Fire Protection Engineering

Corrugated cardboard is widely used in warehouse facilities. The flammable nature of the material, coupled with its ubiquitous presence makes the material a serious fire hazard. As a result, there is interest in developing a universal pyrolysis model that can accurately predict the burning characteristics of the cardboard. Pyrolysis of a double-wall corrugated cardboard was studied in anaerobic and oxygen containing atmospheres using thermogravimetric analysis and a newly developed Controlled Atmosphere Pyrolysis Apparatus (CAPA). The effects of moisture were also examined under non-oxidative conditions. A previously developed cardboard pyrolysis model was demonstrated to reproduce anaerobic gasification. This model was extended to include oxygen diffusion, oxidation reactions, and modified evaporation reactions. The modified model was validated against the mass loss rate data collected in the CAPA at 10.5 vol.% of oxygen and at 2.2 vol.% oxygen with moisturized samples under incident radiant heat fluxes of 20, 40, and 60 kW m^{-2}.

A MODEL FOR NON-OXIDATIVE AND OXIDATIVE PYROLYSIS OF CORRUGATED CARDBOARD

by

Mollie Semmes

Thesis submitted to the Faculty of the Graduate School of the
University of Maryland, College Park in partial fulfillment
of the requirements for the degree of
Master of Science
2013

Advisory:

Professor Stanislav Stoliarov, Chair
Professor Peter Sunderland
Professor Arnaud Trouvé

ACKNOWLEDGEMENTS

Dr. Stanislav Stoliarov deserves the most acknowledgements for the completion of this project. He provided constant guidance and assistance when needed and was a tremendous help. Without his help and encouragement I am positive I would have never finished this project.

Mark McKinnon and Xuan Liu were both immensely helpful. Xuan taught me how to use the lab equipment and was also available to help me fix things when they broke down. Mark helped with almost all aspects of this project. He always made himself available as a sounding board for ideas and deserves a great deal of credit for this project. I would also like to thank Jing Li for his help in the lab and for his suggestions when editing this thesis.

I would also like to thank my family and friends for their support and assistance. My parents always encouraged me and were instrumental in getting me to this point in my life. Emily always forced me to do work even when I really didn't want to and Jean-Luc has been my main source of support and encouragement for the last five years.

My entire lab group has made this last year so much fun and actually made me want to come into the lab every day. Olga Zeller also deserves a lot of thanks for her assistance in the lab, without which this research would have taken much longer.

Lastly, I would like to thank FM Global for their financial support for this research.

TABLE OF CONTENTS

LIST OF FIGURES

LIST OF TABLES

1. INTRODUCTION

1.1 Background

Corrugated cardboard is widely used in warehouse facilities as a way to store goods [1]. Cardboard boxes can be stacked as high as 100 feet and pose a serious fire hazard because of their flammability and proximity to each other [2]. A small fire can quickly spread upwards and transform into a large conflagration due to the extreme combustibility of the goods being stored. Not only is this a hazard in terms of life safety, it can also cost a company millions in damages and lost work. Because of the high costs that can result from even a small incident, it is extremely important that fire protection systems are carefully implemented and that the inherent risk present in warehouse storage conditions be well defined.

Developing a model of cardboard pyrolysis can produce a method for determining the risks and dangers in warehouses without the use of costly full-scale tests. A full-scale model requires a large amount of time, materials, and money, and yields results that cannot always be extrapolated to scenarios different from the one tested. Computer modeling is a much more cost- and time-effective way to predict fire growth and spread [3]. For a computer model to be considered useful, it must be validated against experimental data in order to ensure that it gives accurate predictions. Many researchers use optimization to develop models that fit a set of experimental data. While this method can produce reasonable predictions, the parameters that are optimized are often outside the realm of physical possibility and the results can often not be extended to other sets of data. Obviously, accurately determining the parameters is preferable, but this process is

extremely difficult and there are usually limitations to what can be extracted from bench-scale tests [4]. In order to isolate the needed properties for the computer model used for this research, bench and milligram-scale tests were done on the same corrugated cardboard that was to be evaluated. These experiments were performed in open air. The assumption when developing this model was that the presence of the flame on the sample surface prevented oxidation from occurring. That assumption broke down as the flame died out and only partially covered the surface towards the end of the tests.

In this study, the uncertainty presented by the presence of the flame is removed by conducting the tests at 2.2 and 10.5 vol.% oxygen. This was made possible by the use of a Controlled-Atmosphere Pyrolysis Apparatus (CAPA). The CAPA allows the user to control the atmosphere within which the samples are pyrolyzed. The 2.2 vol.% oxygen condition is the lowest attainable concentration of oxygen in the CAPA, and is meant to simulate anaerobic conditions where oxidation does not occur. The 10.5 vol.% oxygen condition is the highest concentration of oxygen that does not allow the sample to ignite at the highest heat flux tested. This condition is designed to examine the effects of oxidation without the uncertainty introduced by the presence of a flame. The temperature data collected was used to adjust the previously developed model, given that the boundary conditions of the new testing configuration are better defined than those determined for the flaming condition. The mass loss rate data was used to validate the model. The ultimate goal was to develop a comprehensive pyrolysis model that can be applied to any configuration or scenario.

In the development of a comprehensive model, the moisture content of the material is a key component. Warehouses are often in hot environments and the humidity can be high and vary widely. The moisture content of cardboard affects the burning process. In this study, moisture is systematically added to the samples and the samples are pyrolyzed under anaerobic conditions and the data is fit with the pyrolysis model

1.2 Controlled Atmosphere Pyrolysis Apparatus (CAPA)

A Controlled Atmosphere Pyrolysis Apparatus (CAPA) was developed as an addition to the standard cone calorimeter [5]. The CAPA allows the user to pyrolyze small, coupon-sized samples in a specified gas atmosphere. The main benefits of the CAPA are the low cost and risk associated with use. Since the CAPA is able to operate in open air by blowing gas over the sample surface, it is much safer to use than a fully closed device. It is also relatively cheap to construct and operate, being made of only stainless steel cut into variously sized rectangles and aluminum legs. A picture of the CAPA can be seen in Figure 1.

Figure 1. Photographs of the CAPA under the cone calorimeter. The image on the left shows the full device under the cone heater, and the image on the right shows the positioning of the sample within the apparatus.

In this thesis, gasification tests were performed in the CAPA. Gasification tests are experiments conducted in low or non-oxidative conditions [5], so that any possible flame is suppressed. This eliminates the uncertainty introduced by the flame as well as the additional heat flux provided by the flame, and allows the user to examine the kinetics and heat transfer at play in the specified sample. The CAPA has been validated against the NIST Gasification Apparatus at 35 and 50 kW m^{-2} [5] [6].

1.3 ThermaKin

The ThermaKin modeling tool was used to predict the temperature and mass loss rate profiles of the thermal degradation of the corrugated cardboard samples under varying conditions. The model has been validated against both charring and non-charring polymers [7] [8]. ThermaKin is a one-dimensional numerical model that is capable of predicting both pyrolysis and combustion for many different materials [9]. It is especially useful because of its extreme versatility. In ThermaKin, all materials are modeled as a combination of several components arranged in layers. These layers can be comprised of multiple components in different, designated ratios, and can also vary by thickness, composition, and initial temperature. The order of the layers can also be indicated. This allows for the modeling of very complex composites and also allows the user to accurately describe a customized material.

Components are defined by a set of physical properties, including the density, heat capacity, conductivity, and emissivity. The transport coefficient can also be set for each component to indicate how fast or slow gases move through the component. Chemical reactions between components can be specified. The stoichiometric coefficients of each

component, the Arrhenius pre-exponential factor and activation energy, and the heat of the reaction are all used to define the reactions occurring.

The boundary conditions at the top and bottom of the sample can be defined by indicating an external heat flux, a convective coefficient and an ambient air temperature and composition. The heat fluxes and temperatures can both be specified as a function of time if desired. The composition of the environment at the boundary is prescribed by the user. Whether or not the sample will ignite can also be specified.

As with most modeling tools, it is important to be aware of the time step and grid spacing. These can both be specified in ThermaKin and it is up to the user to ensure that appropriate sizes are used.

1.4 Previous Model and Cardboard Kinetics

Corrugated cardboard is primarily comprised of dried cellulosic pulp. Cellulose is made of long chains of glucose molecules [10]. A visual representation of cardboard pyrolysis is shown in Figure 2. The cardboard first undergoes a transition to an intermediary, which is an arbitrary representation of the state between virgin cardboard and char. The intermediary then decomposes further to produce volatile gases and char [11]. In the case of oxidation, the char further degrades into ash.

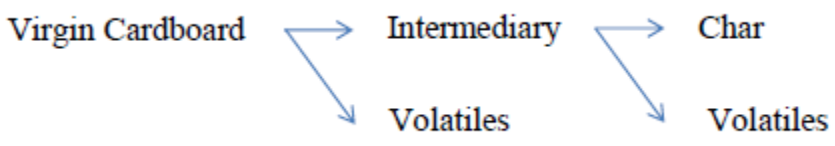

Figure 2. Decomposition process of corrugated cardboard.

A model was previously developed under flaming conditions. Bench-scale tests were conducted in a cone calorimeter. 10 by 10 cm samples of corrugated cardboard were pyrolyzed under heat fluxes ranging from 20 to 80 kW m^{-2}. Temperature and mass loss rate profiles were recorded. A key assumption in this model was that the flame prevented oxidation from occurring. In order to develop the Arrhenius parameters, thermogravimetric analysis TGA data was used. The corrugated cardboard samples were finely ground and gasified in nitrogen in a TGA system. Reactions were fit to the mass loss rate curves in order to develop a comprehensive reaction scheme [12]. The main objective was to create a reaction scheme that captured all of the behavior of corrugated cardboard in the simplest way possible. The end result was a reaction mechanism that consisted of four, first-order reactions: the three seen in Figure 2, as well as a reaction governing the evaporation of water from the virgin cardboard. These reactions were fitted using the Arrhenius pre-exponential factor (A) and activation energy (E), as well as the stoichiometric coefficients of the solids and gases in each reaction. The heat capacities were determined using DSC data.

Several simplifying assumptions went into the development of this model. The reactions discussed above represent the most simplistic way to capture all the behavior of the normalized mass loss rate profile [12]. This reaction mechanism does not accurately capture all of the chemistry occurring during pyrolysis; however it is a simple way to represent the TGA data and production of volatiles accurately. The reactions do not necessarily represent what is actually occurring, however, there is evidence that the selected reaction scheme has merit. Several other researchers have used a similar or identical reaction scheme to model cellulose pyrolysis. Researchers in France conducted

tests on cardboard using thermogravimetric analysis in an attempt to develop a universal reaction scheme that would govern the material degradation [11]. They performed tests at three different heating rates in 100% nitrogen and found that the heating rate had an effect on the reaction scheme to describe the mass loss rate. In order to develop one reaction scheme that would best describe the mass loss rates taken at each heating rate, several schemes were considered. In total, six reactions schemes were evaluated and Arrhenius parameters were fit to the mass loss curves for each heating rate, resulting in eighteen different sets of Arrhenius pairs. The Arrhenius pairs were assumed to be constant throughout the entire experiment. The first reaction scheme described the degradation of cardboard from virgin cardboard to volatiles and the intermediary, and then the intermediary to more volatiles and char. This reaction scheme most closely resembles the one used in ThermaKin to model the experiments presented in this thesis that were done under anaerobic conditions. The chars described in the ThermaKin model were further broken down into an initial char and a final char.

Although none of the reaction schemes produced a completely accurate fit, the first reaction scheme discussed above was shown to have the best fit of all the data without discontinuities in the curve caused by numerical divergences, and was thus selected as the universal scheme to describe the degradation of the cardboard in nitrogen. The other five reaction schemes were variations on the first scheme, and included up to two forms of the intermediary and the virgin cardboard. In several of the reactions, the two forms of the intermediary or virgin cardboard were pyrolyzed in parallel reactions, although reactions where they pyrolyzed in sequence were also explored. Although the first reaction scheme presented in this paper was selected, the authors came to the conclusion that statistical

analyses of the accuracy of the fits of each of the reaction schemes were so close that no reaction scheme could definitively be considered the best. This implies that there are multiple ways that the degradation of cardboard can be modeled.

The two conditions under which samples are pyrolyzed in this thesis represent a little to no oxidation scenario and an oxidation scenario without the presence of a flame. These two conditions are driven by different mechanisms. The first scenario, which is discussed above, corresponds to forced pyrolysis, where the degradation and gasification is driven by the imposed external heat flux [13]. Any material, when exposed to a sufficient heat flux, will experience degradation, even without sufficient oxygen in the atmosphere to support flaming combustion or smoldering. The second scenario is most accurately described by the smoldering process. It is driven by the diffusion of oxygen from the surface of the sample. The oxygen attacks the surface of the sample and facilitates the degradation of the sample, resulting in the production of carbon dioxide and carbon monoxide as well as other products of combustion [13].

Both types of pyrolysis have been studied in many cellulosic materials, including cardboard, mostly as a way of assessing the possibility of using incineration as a way of dealing with waste. Cardboard comprises 30% of the solid waste in landfills, and given the low production of volatiles that occurs from cardboard combustion, burning the waste presents a viable option, especially in developing countries [11] [14]. Several researchers have studied the combustion of cardboard as a way of determining an appropriate way to eliminate the waste.

Researchers at the University of Maryland performed experiments on cardboard in inert and oxidative environments [14]. Differential scanning calorimetry (DSC) and thermogravimetric analysis (TGA) were used. Samples of finely ground cardboard containing 5% moisture were gasified in argon, oxygen, air, and argon with air added at 600 ºC. Each of these four environments was tested at heating rates of 10 and 50 K min^{-1}. Arrhenius parameters were calculated for each scenario. The researchers found that the heating rate of the TGA and DSC as well as the gas atmosphere affected the gasification characteristics and calculated Arrhenius pairs. The authors concluded that the differences caused by the heating rates could not be fully explained by differences in heat transfer through the sample, and mass transfer must also play a role. A physical manifestation of these differences may be observed in the char yields. The researchers observed that the char yields in the inert environments were higher when compared to the oxidative environments with the same heating rates, which is logical, as the char oxidizes, but they also observed that a slower heating rate resulted in a lower char yield for all material and gas environments examined. The authors suggested that this could be attributed to the evaporation of liquid tar that develops during pyrolysis. This evaporation is strongly dependent on the heating rate.

The heating rate is shown in several papers to have an effect on the kinetics of cellulosic materials [11] [14] [15]. Another of the simplifying assumptions that went into the development of the original model presented above was that the differences in the heating rate were not accounted for [16]. A heating rate of 10 K min^{-1} was used in the TGA to collected data on the finely ground corrugated cardboard. Several slower heating rates were also tested, but there was not found to be a significant difference in the mass loss

rate profiles. Higher heating rates were not tested in the TGA, because of the porous nature of the cardboard; the researchers assumed that heat transfer gradients would develop in the sample crucible, creating undesirable testing conditions. However, the cone calorimeter tests conducted do produce extremely high heating rates within the sample, and those results have been validated against the model developed in the TGA at the low heating rates, so the model has been shown to be valid at higher heating rates.

The above reaction scheme was modified to create a universal reaction scheme that represented all oxidative and non-oxidative atmospheres. The new reaction scheme was developed in a similar manner to the original, anaerobic scheme, by using TGA data. Finely ground corrugated cardboard was pyrolyzed in the TGA at 10 and 21 vol.% oxygen. A universal reaction mechanism was developed that provided the best fit of the data. It was possible to better fit the mass loss rate curves at each oxygen concentration by using different reaction parameters for each concentration, but this undermined the purpose of the study, which was to develop a universal model for the pyrolysis of corrugated cardboard. The oxidative reaction scheme is shown in Table 1.

Table 1. The previously developed oxidative reaction scheme of corrguated cardboard.

#	Reaction Equation	A (sec^{-1})	E_a (J/mol)	h_r (J g^{-1})
1	$H_2O_\ell \rightarrow H_2O_g$	6.14	2.35×10^4	-2.5×10^3
2	$CB_a \rightarrow 0.9CB_b + 0.1CB_{volatiles}$	7.95×10^9	1.3×10^5	0
3	$CB_b \rightarrow 0.37CB_{char,1} + 0.63CB_{volatiles}$	2.0×10^{11}	1.6×10^5	-1.3×10^2
3a	$CB_b \rightarrow 0.59CB_{char,1} + 0.41CB_{volatiles}$	$4.76 \times 10^9[O_2]$	1.6×10^5	0
3b	$CB_b \rightarrow 0.48CB_{char,1} + 0.52CB_{volatiles}$	$1.11 \times 10^{21}[O_2]$	2.8×10^5	0

4	$CB_{char,1} \rightarrow 0.59CB_{char,2} + 0.41CB_{volatiles}$	2.61×10^{-2}	1.7×10^{4}	0
4a	$CB_{char,1} \rightarrow 0.48CB_{char,2} + 0.52CB_{volatiles}$	$1.24 \times 10^{-3}[O_2]$	1.7×10^{4}	0
4b	$CB_{char,2} \rightarrow 0.15\ ash + 0.85CB_{volatiles}$	$2.31 \times 10^{125}[O_2]$	1.69×10^{6}	0

This new reaction scheme incorporates four additional oxidation reactions. The first two oxidation reactions (corresponding to reactions 3a and 3b in the table) occur in parallel with the second decomposition reaction (reaction 3). These reactions speed up the decomposition reaction. The third oxidation reaction (reaction 4a) is in parallel with the second decomposition reaction (reaction 4). The fourth oxidation reaction is in sequence and works to reduce the final residue yield by converting the char to ash.

1.5 Oxidation and Smolder

Smoldering is defined as a slow combustion process that occurs without the presence of a flame. Smoldering often occurs when there is not enough heat or oxygen to support flaming combustion. Smoldering can be incredibly dangerous because it can go undetected inside a material for long periods of time, and can lead to flaming when enough heat is added. This combination can create situations where materials can smolder undetected for days or weeks until eventually catching fire. The smoldering process also produces large amounts of smoke and toxins.

As mentioned in the previous section, smolder is driven by the diffusion of oxygen from the sample surface into the sample. Oxidation occurs at the sample surface as the oxygen attacks the sample and aids in the degradation of the material. In general, the greater the increase in the concentration of oxygen at the sample surface, the faster the smolder front

will propagate and the hotter it will burn [13]. Researchers at the National Bureau of Standards (now NIST) conducted tests on white pine at 0, 10.5, and 21% oxygen [17]. They found that the presence of oxygen significantly increases the mass loss rate of the sample. At 40 kW m^{-2}, the peak mass loss rate at 21 vol.% oxygen was double the peak mass loss rate of the sample in 0 vol.% oxygen. The sample that was pyrolyzed at 10.5 vol.% oxygen had a peak mass loss rate approximately in the middle of the other two atmospheric conditions. The average mass loss rate at 25 kW m^{-2} was three times larger in 21 vol.% oxygen than in 0 vol.% oxygen. The NIST results also showed that the temperature was as much as 200 ºC higher in the 21 vol.% oxygen experiments as opposed to the anaerobic pyrolysis. The researchers also observed higher CO and CO_2 yields as the concentration of oxygen increased. Researchers at the University of California at Berkeley used a pyrolysis model to attempt to model the results of this research [18]. They assigned exothermic heats to the oxidative reactions due to the increase in temperature seen by previous researchers at higher oxygen concentrations.

Researchers at FM Global performed similar research on cardboard in a Fire Propagation Apparatus (FPA) [19]. Tests were conducted in 2, 6, 8, 10, and 14 vol.% oxygen at 20, 60, and 100 kW m^{-2}. The results show that at 20 kW m^{-2}, the average and peak mass loss rates significantly increase as the oxygen concentration increases. However, at the higher heat fluxes, the difference between the mass loss rate profiles at the different oxygen concentrations is negligible. The authors attribute this difference between the pyrolysis of wood and cardboard to the significant structural differences between the two materials. While both are lignocellulosic materials, their structure and kinetic properties are very different. The authors hypothesize that the heat released by the oxidation of the char is

small in relation to the radiant heat flux on the sample, and the effect of the oxidation is less noticeable as the heat flux increases. The researchers also suggest that there may be an upper limit to the heat released by the oxidation of the char because the controlling element in the process is the diffusion of oxygen through the char. Unlike the mass loss rate profiles, the surface temperature profiles increase as the oxygen concentration increases. These increases are definitely most noticeable at the lowest heat flux, but are evident at the two higher heat fluxes as well. The researchers noticed that the temperature profiles for each heat flux were nearly identical at all oxygen concentrations for the early stages of pyrolysis, indicating that the exotherm associated with the reactions between the oxygen and the un-burned cardboard is small. The researchers also observed that the increased presence of oxygen encourages the production of char. At higher heat fluxes, the external heat is so high that the virgin material is rapidly converting to char anyway, so the effect of the increased oxygen concentration is not noticeable. This explains the similar mass loss rate profiles at the higher heat fluxes as well as the increase in the temperature profiles as additional heat fluxes are added onto the surface due to the oxidation of the char.

1.6 Moisture Content

In this thesis, experiments are presented where moisture has been uniformly added to the cardboard samples, which are then gasified under anaerobic conditions. A few researchers have studied the effect of moisture on the pyrolysis of biomass and cellulosic materials. They concluded that the presence of water changes the kinetics of the material. Researchers in Shanghai performed tests on rice straw, using TGA and DSC analysis. They tested rice paper with moisture contents of 13.45, 16.6, and 21.4 % moisture

content. And found that the char yields decreased as the moisture content increased, from approximately 28% to 9% from the lowest to highest moisture content [20]. Researchers at the University of Sheffield performed similar experiments on municipal waste with different moisture contents and found similar results [21]. The researchers observed that the higher the moisture content, the higher the char burning rate. This result was coupled with a decrease in char formation as the moisture content increased. The two effects combined to produce a decrease in the char yield as the moisture content increased. A possible explanation for these observed phenomena is that the moisture would increase the amount of volatiles leaving the wood and would also increase the production of tars and volatile gases, while reducing the residence time the volatiles spent in the material which in turn would reduce the char yield [22].

2. EXPERIMENTAL

2.1 Material

The corrugated cardboard samples used in all of the experiments presented in this thesis were double-walled with three linerboard layers and two flute layers in between the linerboards. The samples had a designation of 69-23B-69-23C-69. This designation represents the density of each layer in pounds per feet-squared. The first number indicates the top linerboard layer, followed by the B-flutes layer, and so on. A side-view schematic of the cardboard is shown in Figure 3.

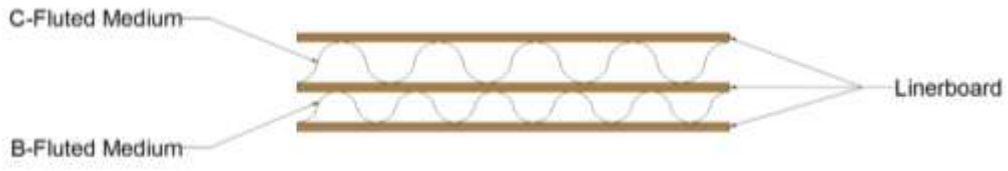

Figure 3. Corrugated cardboard side-view schematic.

The linerboards all have the same thickness of .64 ± .03 mm, while the C and B-flutes have a thickness of 3.4 ± .2 mm and 2.1 ± .2 mm respectively.

For the tests, the corrugated cardboard was cut into 80 by 80 mm sample squares. These samples were placed in a desiccator with Drierite for at least two days prior to being tested to remove as much moisture as possible and ensure the uniformity of the samples. The moisture content after drying was found to be approximately 2%.

2.2 Controlled Atmosphere Pyrolysis Apparatus

The Controlled Atmosphere Pyrolysis Apparatus (CAPA) was integrated into a standard cone calorimeter [23] to allow the user to perform gasification tests on small samples in a

specified gas environment. A detailed drawing of the CAPA is shown in Figure 4. The basic design of the apparatus consists of two concentric metal square ducts. The sample is placed on a holder within the inside square. The desired combination of gases is flowed between the inner and outer duct, though small glass beads 4-5 mm in diameter to even out the flow. The gas flows straight upwards through the ducts and settles on top of the sample. In this manner it is possible to create stable, non-atmospheric conditions.

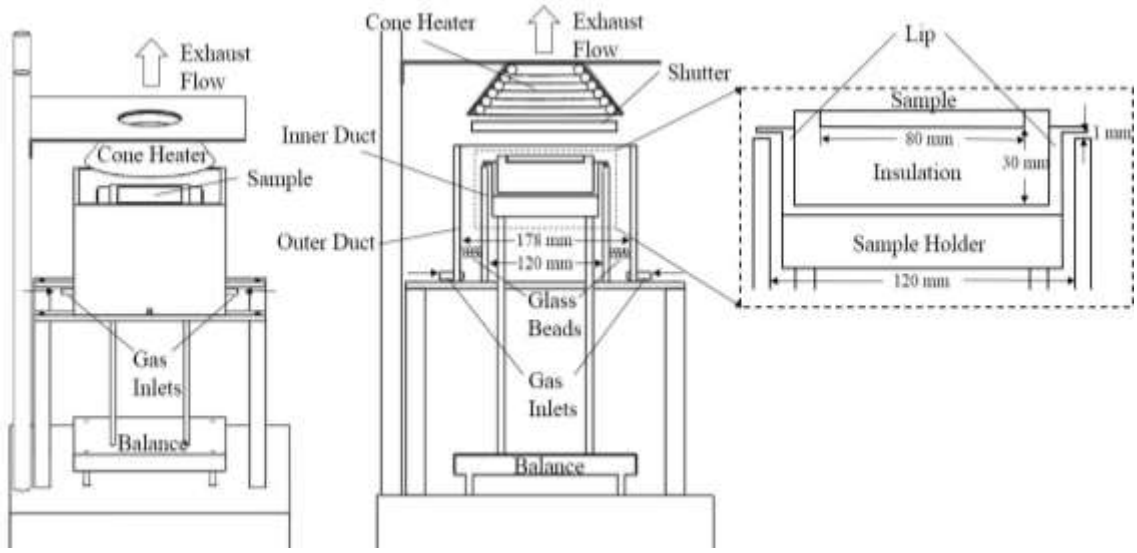

Figure 4. Scaled drawing of the CAPA.

A stainless steel sample holder was placed within the inner duct so that the sides of the holder did not touch the apparatus. This allowed the user to place the sample holder on a scale to get mass readings during gasification tests without interference from the CAPA. The sample was placed in the holder on top of insulation, underneath the cone heater. An air-tight door in the side of the CAPA allowed the user to easily place the sample holder on top of an aluminum mount with legs that rest on the balance. The sample holder has a lip around its top edge that, when placed on the mount, rested 1 mm above the top of the

inner duct. This prevented gases from escaping through the bottom of the CAPA while still ensuring that the apparatus did not interfere with mass readings.

The corrugated cardboard was cut into 80 by 80 mm samples. In order to prevent radiation from the cone heater from heating the sides of the sample, a 10 mm thick border of Kaowool PM was cut and the sample was placed inside the insulation. More Kaowool PM was cut into 100 by 100 mm samples and stacked 28 mm thick and placed inside the sample holder. The sample wrapped in Kaowool was then placed on top of this insulation. When inserted onto the aluminum mount, the sample rested 40 mm below the cone heater.

A Schmidt-Bolter heat flux gauge was used to set the heat flux. The CAPA was removed from the area under the cone heater and the gauge was placed at the height of the sample in the center, 40 mm under the heater. Since the sides of the outer duct of the CAPA are taller than the sample, it was thought that the heated metal might contribute some heat to the sample surface. In order to determine the uniformity of the heat flux across the sample surface, the heat flux gauge was placed at 25 evenly spaced points over the plane where the top of the sample would be located during a test. The cone heater was set to 50 kW m^{-2} in relation to the standard position at the center of the sample surface. The heat flux was measured at each of the 25 points on the sample surface. The uniformity was calculated to be 96%; therefore, it was decided that the effect of any radiation from the hot metal outer wall could be ignored.

The total flow of gas was set at 225 SLPM by an ALICAT MCR series mass flow controller. The total flow was comprised of combinations of air and nitrogen. For the

2.2 vol.% oxygen tests, the entire flow was nitrogen. For the 10.5 vol.% oxygen tests, 90 SLPM of air and 135 SLPM of nitrogen were used. The volume percentage of oxygen at the sample surface was determined by setting up the CAPA underneath the cone heater with a piece of Kaowool PM in place of a cardboard sample, setting the cone to the desired heat flux, and running the desired combination of air and nitrogen through the CAPA for two minutes to allow the gases to equilibrate. The atmosphere was sampled 1 mm above the sample surface in nine places evenly distributed across the sample surface and the concentration of oxygen was analyzed using a Servomex 4100 gas analyzer. The concentration of oxygen was measured at 20, 40, and 60 kW m^{-2}. The concentration varied only slightly for each different heat flux, so the average value over all tests was used. The lowest attainable concentration of oxygen was 2.2% ± .4 by volume.

The temperature was measured in the middle of the top and bottom linerboard, 38 mm from the edge. A pilot hole was made in the liner boards with a needle and two K-type thermocouples were inserted. The length of the needle dictated the depth of the thermocouple bead. The sample with attached thermocouples was inserted into the Kaowool border and placed on top of a piece of aluminum foil in the holder. The thermocouples were attached to a NetDaq and temperature measurements were recorded in LabView. The CAPA apparatus was set up in the standard way described above with the apparatus allowed to heat under the cone heater for 5 minutes and the gas flow allowed to run for two minutes before testing started to ensure the apparatus reached equilibrium. After the CAPA was set up, the radiation blocking shutter was put into place, and the holder with the sample and thermocouples was inserted into the apparatus. The shutter was removed and the temperatures were recorded in both the thermocouples.

This test was repeated at 20, 40, and 60 kW m^{-2}. Three to five tests were done at each heat flux at both the anaerobic and the oxidative conditions.

The mass loss rate was measured under the same standard conditions discussed above at 20, 40, and 60 kW m^{-2}. The sample was placed in the border and on top of a piece of aluminum foil. The foil rested on top of the back insulation. The scale was calibrated and zeroed before each set of tests. After the scale was zeroed, the sample holder was placed inside the CAPA and the shutter was opened, starting the mass measurements. Five of these tests were performed at 20 kW m^{-2} and three were performed at 40 and 60 kW m^{-2} in both the anaerobic and oxidative pyrolysis conditions to compensate for the greater experimental scatter seen at 20 kW m^{-2}.

2.3 Moisture Content

In order to examine the effects of moisture during anaerobic pyrolysis, the moisture content was systematically increased. In order to do this, the samples were first dried in the same manner utilized for all the samples. After being dried, the samples were weighed and placed in an airtight Tupperware container that contained a Petri dish filled with water. The container was placed in a warm environment heated to approximately 30 C for 48 hours. Immediately before tests were performed, the container with samples and the Petri dish were placed in an oven at 45 C for 8 hours. This resulted in a moisture content of 12.6 ± .6 %. These steps were taken to mimic conditions that could be found in a warehouse on an extremely hot and humid day. The samples were then weighed again and used for testing immediately. The moisture content was found by subtracting the new weight of the sample from the previously measured, dried weight and divided by

this original weight. In order to assure that the same amount of moisture remained in the sample at the start of the test, the process of placing the sample in the holder and setting up the CAPA apparatus for each test was carefully practiced and timed. It was determined that the preparation of the sample took two minutes. A sample was removed from the conditioning box and immediately weighed. The sample was then allowed to sit at ambient temperatures for two minutes and weighed again. The process was repeated three times to find the average amount of moisture lost during the test preparation. This amount was subtracted from the weight of the sample after being taken out of the conditioning box.

3. EXPERIMENTAL RESULTS

3.1 Non-Oxidative Pyrolysis

The temperature profiles were used to parameterize the pyrolysis model and thus it was extremely important that the measured data be consistent and repeatable. The average measured temperature profiles for the anaerobic condition are shown with error bars representing two standard deviations away from the mean in Figure 5.

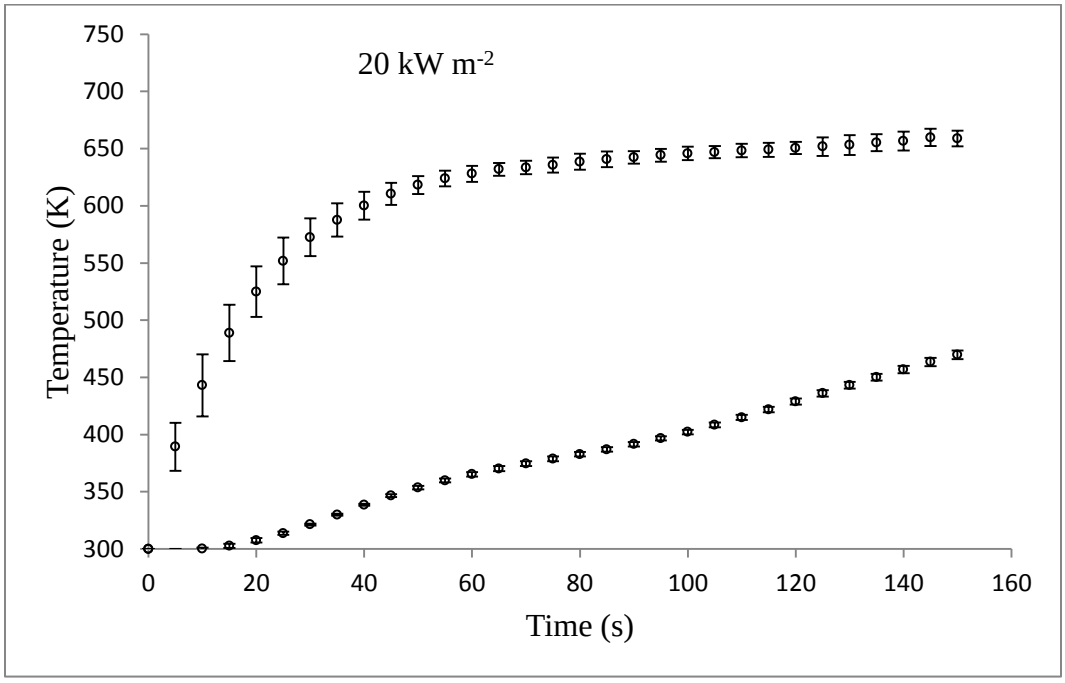

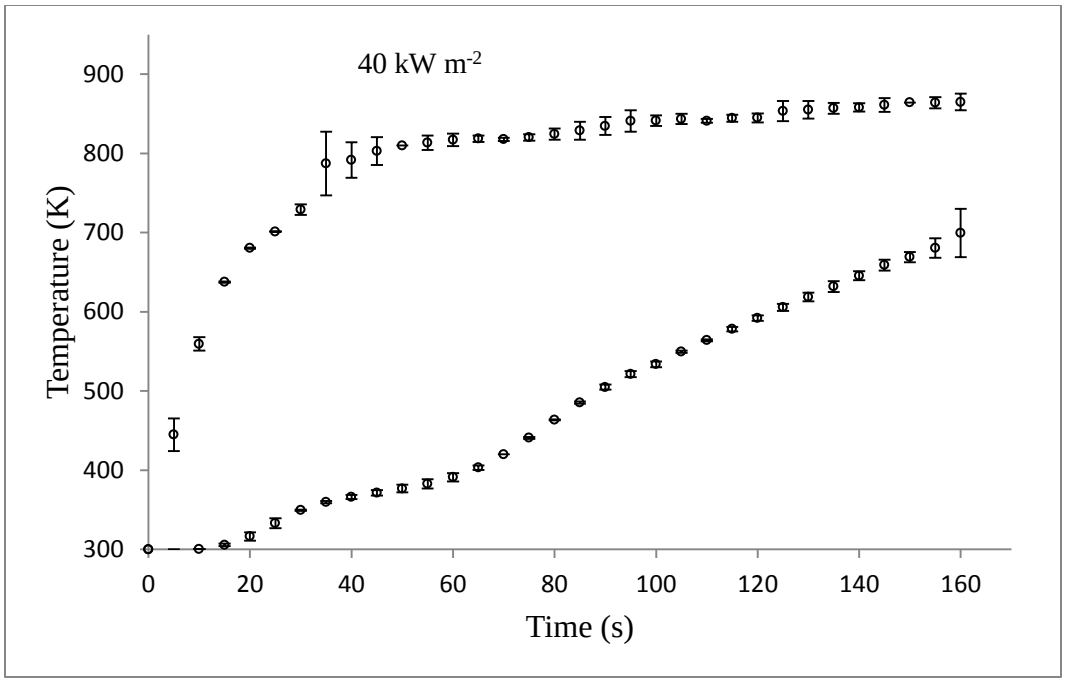

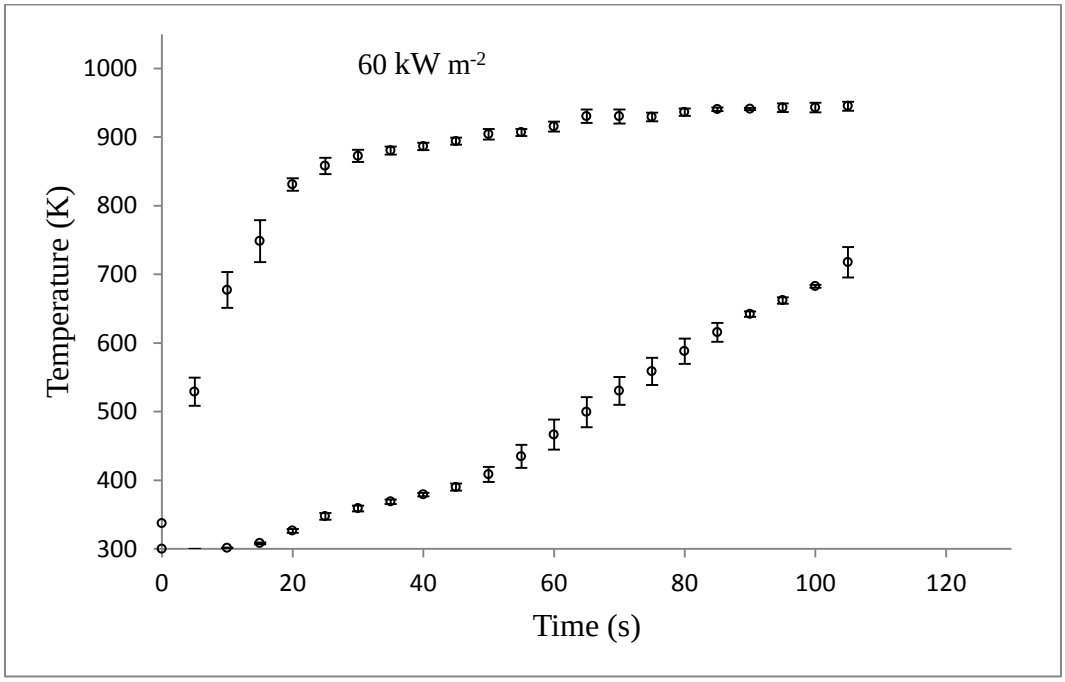

Figure 5. Temperature profiles collected in non-oxidative conditions with error bars representing two standard deviations from the mean.

The average standard deviation normalized by the mean value of the temperature data was 1.1%, .95%, and 1.5% at 20, 40, and 60 kW m^{-2} respectively. The average values can be broken down into the average values for the top and bottom linerboards. At 20 kW m^{-2}, the normalized standard deviation was 1.6% and .6% for the top and bottom linerboards respectively. At 40 kW m^{-2}, the normalized standard deviation was 1.1% and .8% respectively, and at 60 kW m^{-2}, 1.2% and 1.8% respectively. The standard deviations of the lower linerboard temperatures were generally smaller than those of the top linerboards, although the normalized standard deviations were comparable because of the higher values of the top linerboard temperatures.

The average mass loss rate is shown in Figure 6 with error bars representing two standard deviations. The lower the external heat flux, the higher the scatter. Five tests were done at 20 kW m^{-2} and three at 40 and 60 kW m^{-2} in order to compensate for this.

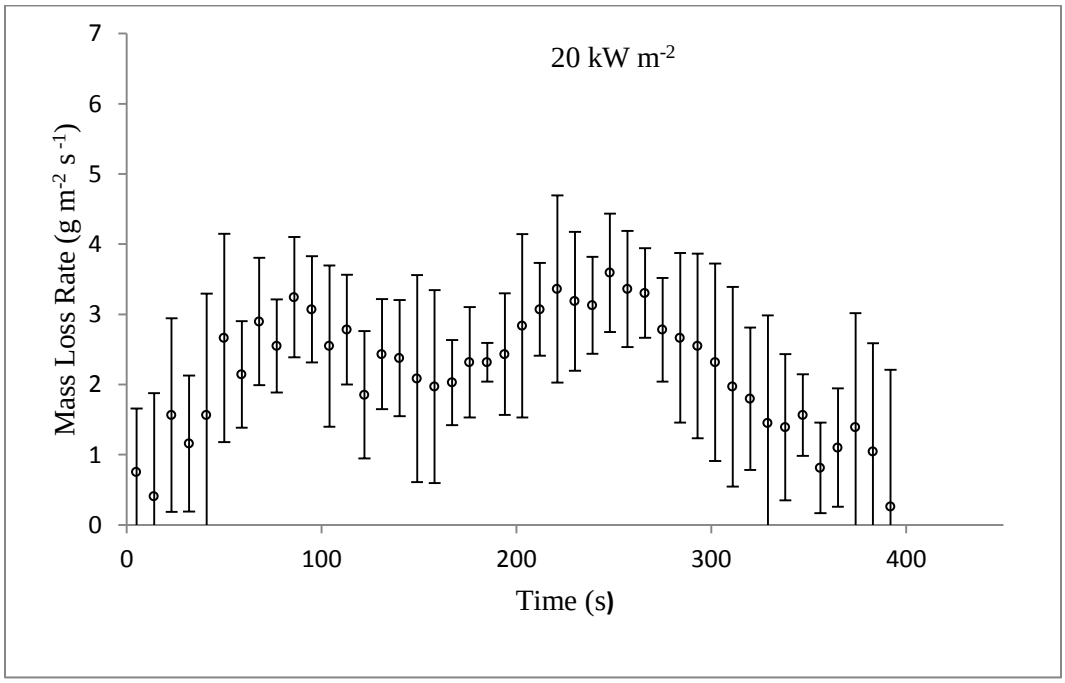

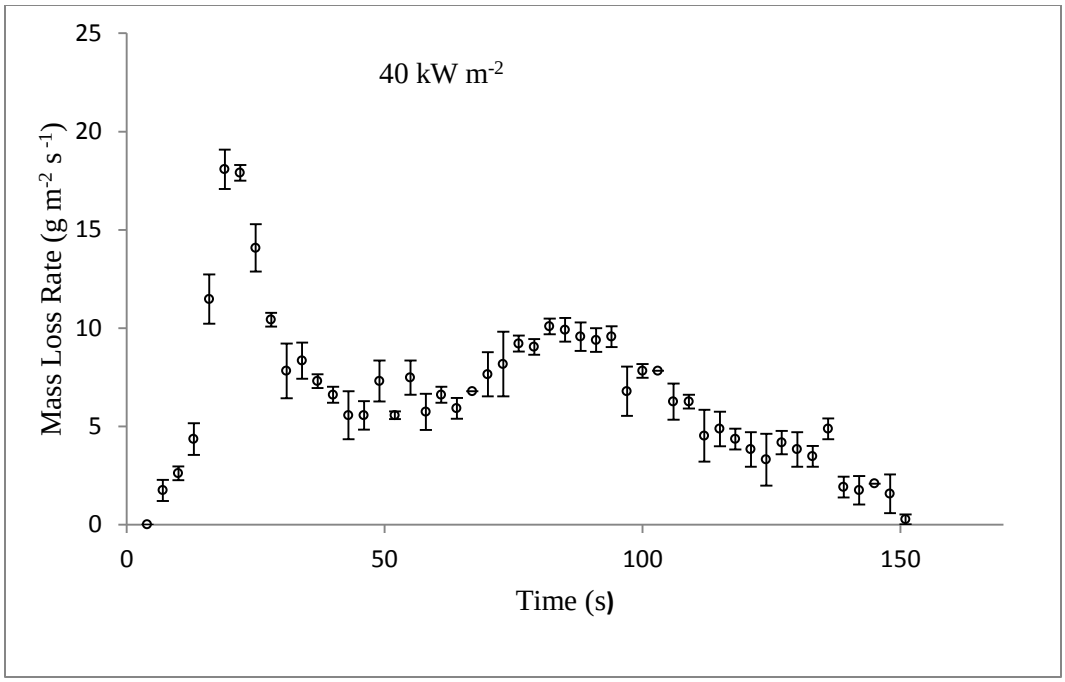

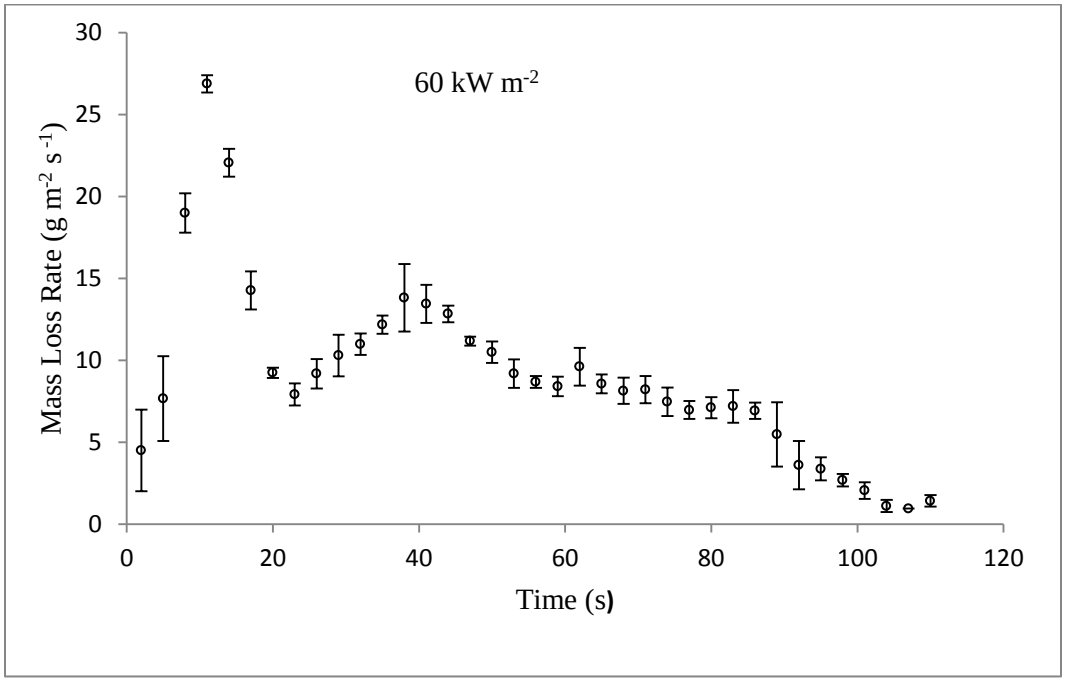

Figure 6. Mass loss rate profiles collected under anaerobic conditions with error bars representing two standard deviations from the mean.

The average error, represented by two standard deviations away from the mean, was .7, .7, and .9 for 20, 40, and 60 kW m^{-2} respectively. The average error as a percentage of

the mean value was 38, 15.5, and 13% for 20, 40, and 60 kW m^{-2} respectively. The error bars in the plots represent two standard deviations away from the mean, as was the case in the temperature tests. The standard deviations were much larger in the mass loss rate tests than the temperature tests due to the nature of the tests done. The variation in the mass loss rate data was not as important as in the temperature data, since the temperature data was used to fit the model, and the mass loss rate profiles were simply used as validation for the model. As discussed above, the scatter for the 20 kW m^{-2} test was much larger compared to the higher heat flux tests. The reason for this is most likely that the scatter caused by the gas flowing over the sample, as well as normal experimental error, was much more pronounced at the lower mass loss rates. Two extra tests were done at 20 kW m^{-2} to compensate for this.

3.2 Oxidative Pyrolysis

The temperature profiles of the top and bottom linerboard are shown in Figure 7 for the samples pyrolyzed at an average 10.5 vol.% oxygen. The normalized error is .8%, 1.3%, and 1.3% at 20, 40, and 60 kW m^{-2} respectively. The error on the top and bottom linerboards is very similar.

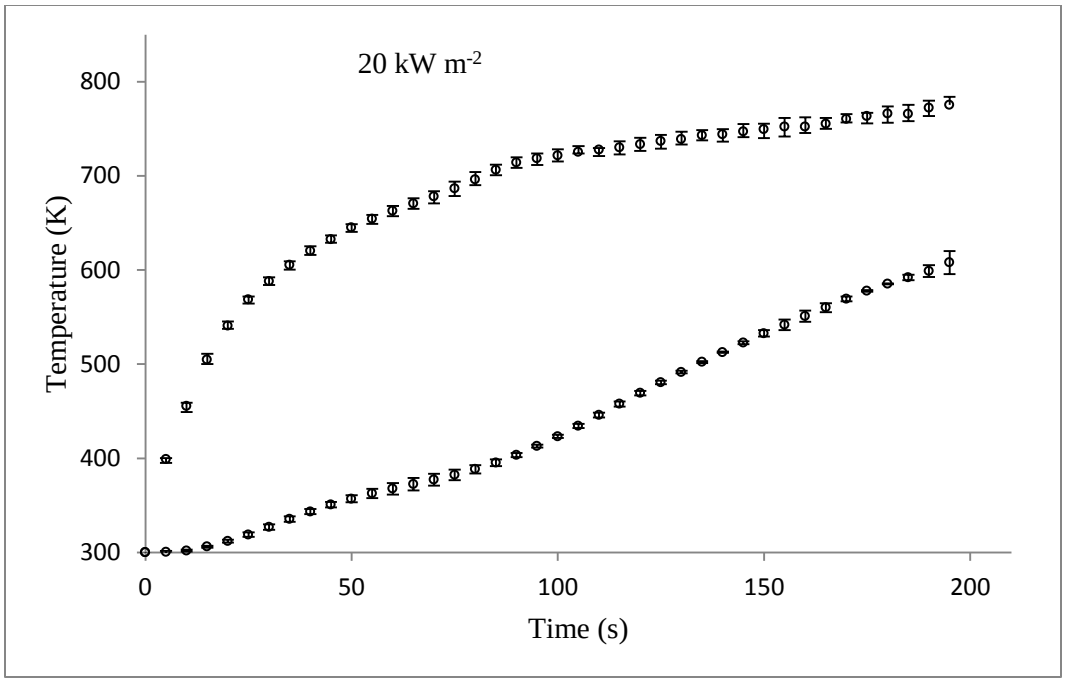
20 kW m-2
Temperature (K)
800
700
600
500
400
300
0
50
100
150
200
Time (s)

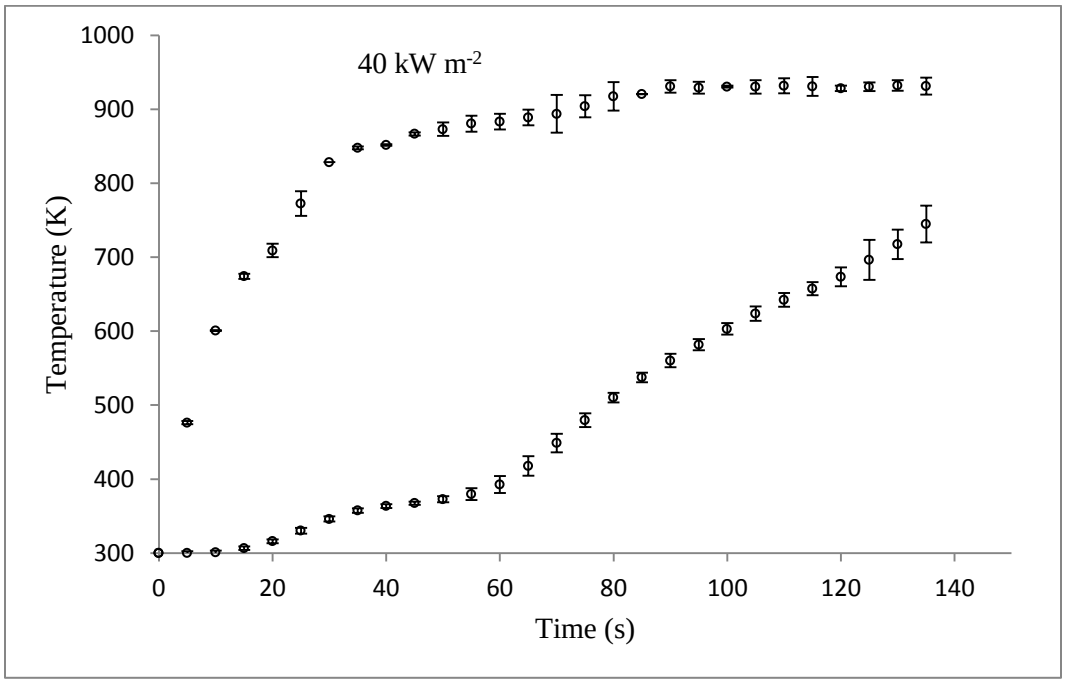
40 kW m-2
Temperature (K)
1000
900
800
700
600
500
400
300
0
20
40
60
80
100
120
140
Time (s)

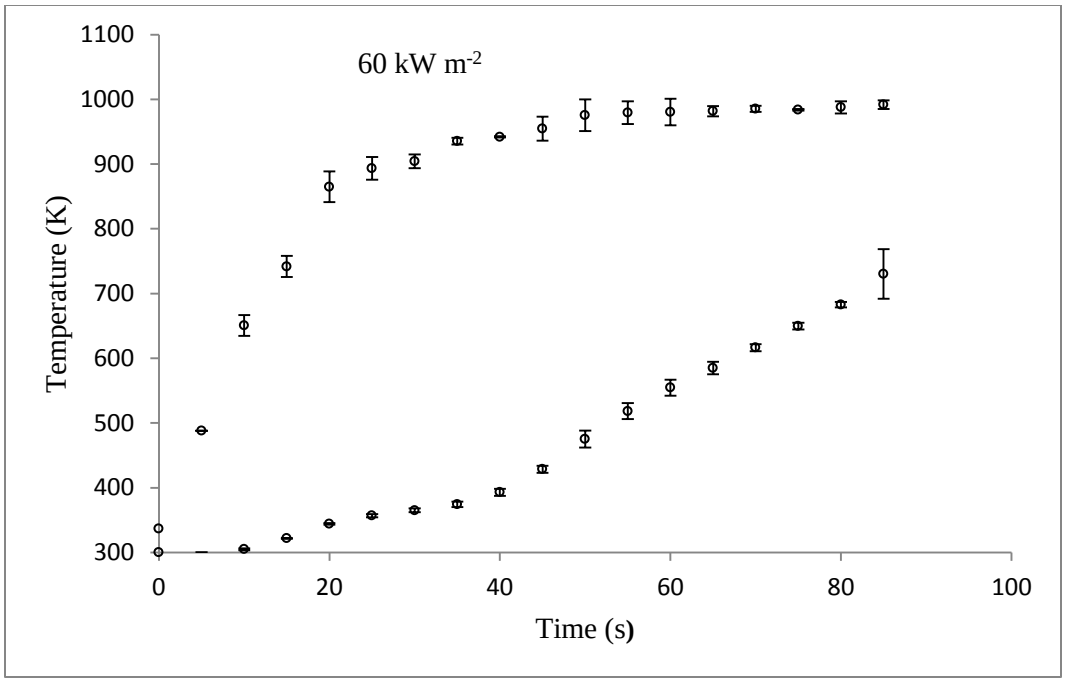

Figure 7. Temperature profiles collected under oxidative conditions (10.5 vol.% oxygen) with error bars representing two standard deviations from the mean.

The mass loss rate profiles at each flux with the experimental error are shown in Figure 8. The normalized standard deviation is 43, 27, and 14.5% at 20, 40, and 60 kW m^{-2} respectively. The oxidative mass loss rate exhibited the same behavior as the non-oxidative data presented above. The scatter decreased as the heat flux increased. Again, more tests were done at the lowest heat flux to compensate for this trend.

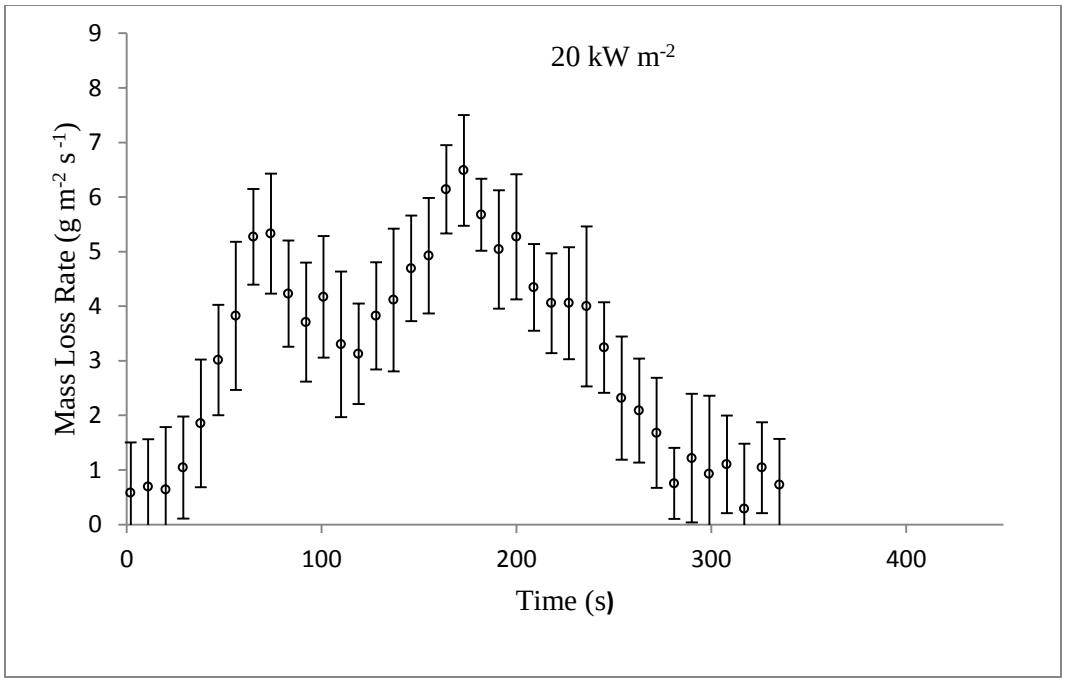
20 kW m-2
Mass Loss Rate (g m-2 s-1)
Time (s)
0
1
2
3
4
5
6
7
8
9
0
100
200
300
400

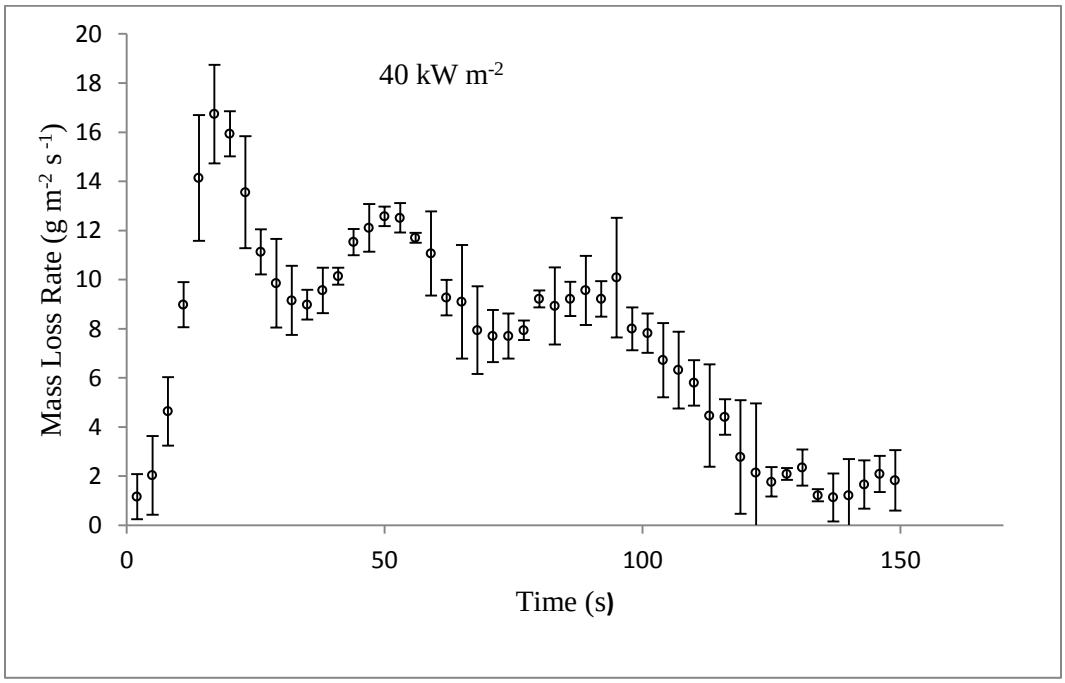
40 kW m-2
Mass Loss Rate (g m-2 s-1)
Time (s)
0
2
4
6
8
10
12
14
16
18
20
0
50
100
150

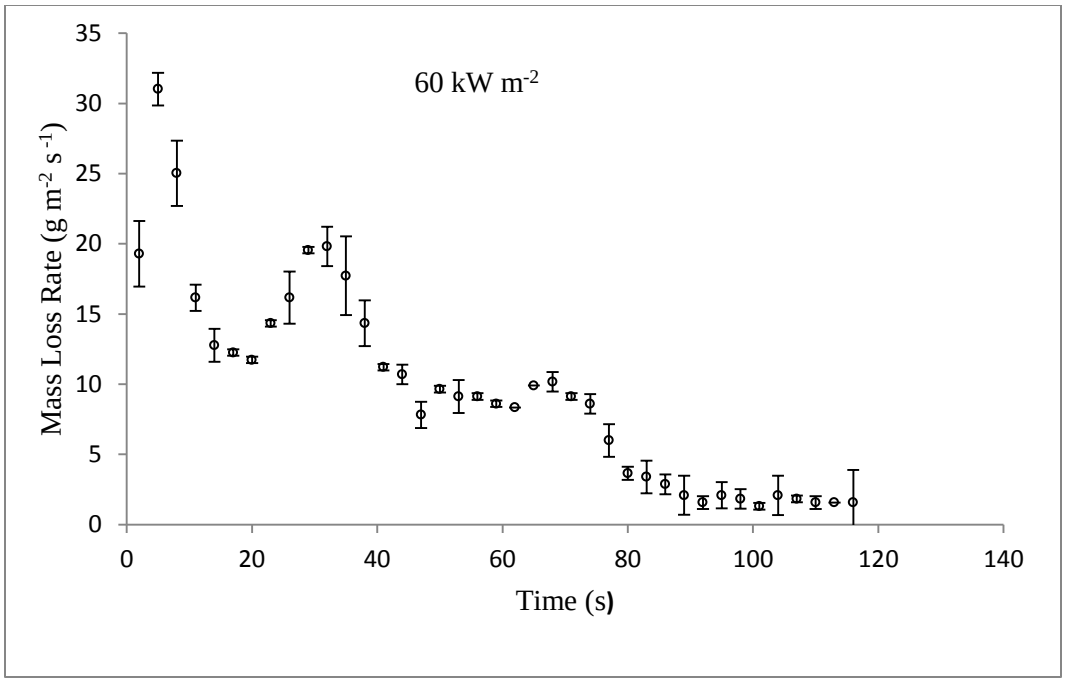

Figure 8. Mass loss rate profiles collected under oxidative conditions (10.5 vol.% oxygen) with error bars representing two standard deviations.

3.3 Moisture Content

A big challenge when performing tests with high moisture content is making sure that all the samples are uniformly moisturized. This presented a twofold challenge. The corrugated cardboard samples must be evenly exposed to the water vapor and must also be prepared in the same amount of time. After removing the samples from the conditioning box, the moisture immediately started to evaporate. The experimental section above discusses how this problem was dealt with. The conditioning process resulted in samples containing 12.6 ± .6 % moisture. The temperature profiles of the moisture samples at each heat flux are shown in Figure 9. The normalized error is 1.1%, 6.4%, and 2.4% at 20, 40, and 60 kW m^{-2} respectively. The temperature error is notably

larger for the moisturized samples. This is most likely due to the differences in the moisture content from sample to sample, adding to the experimental error.

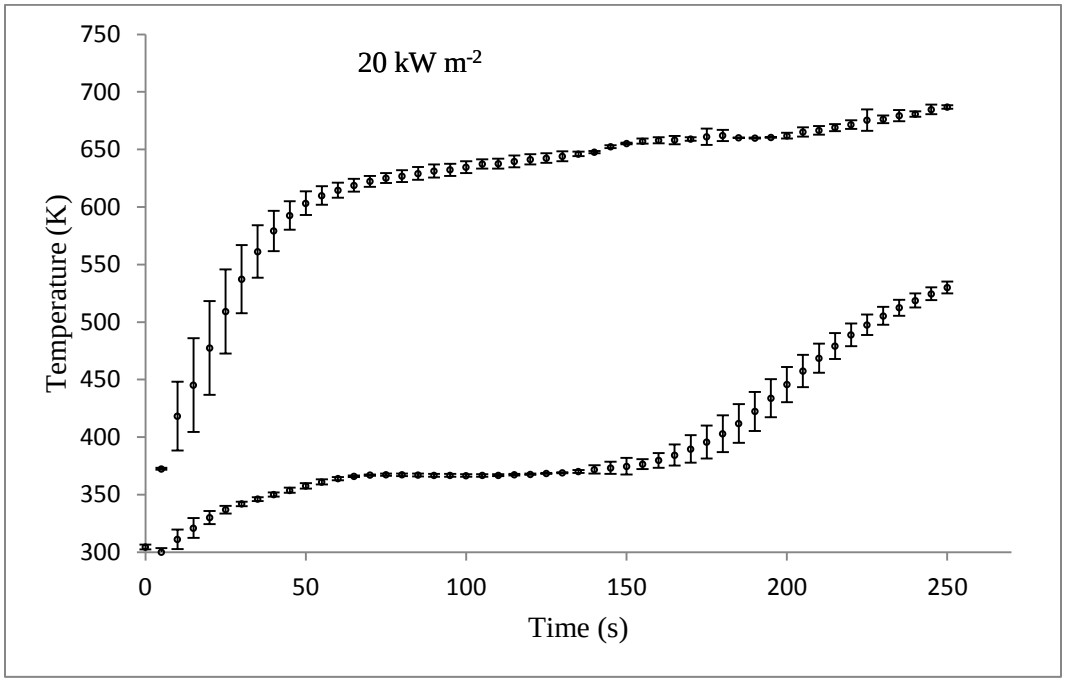

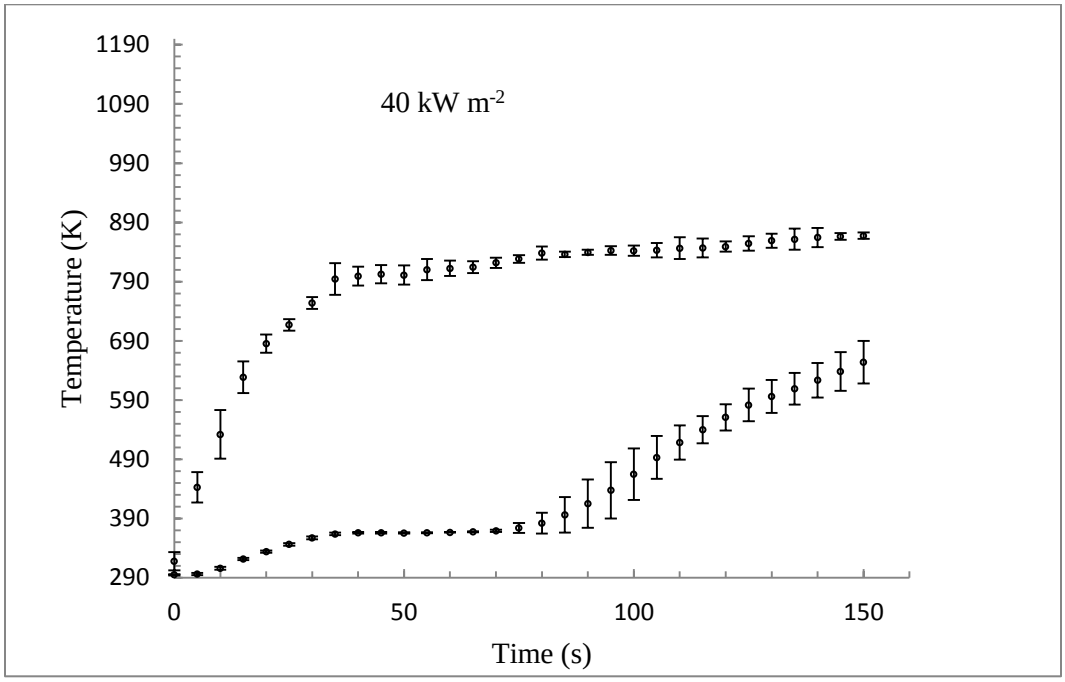

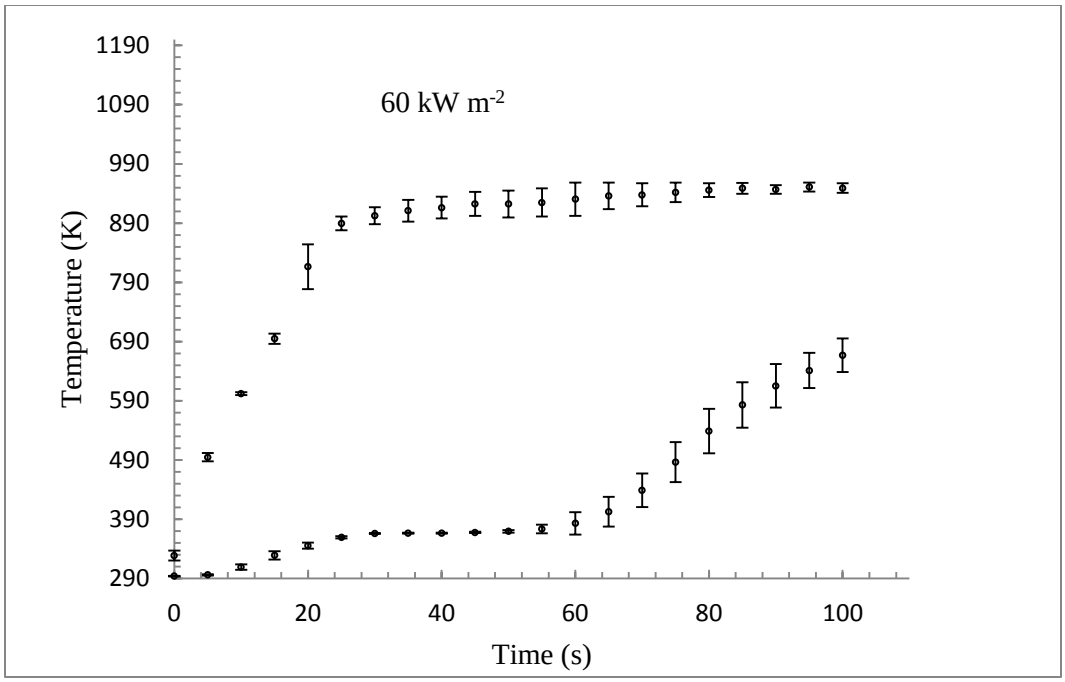

Figure 9. Temperature profiles of samples with added moisture (12.6% water) collected under anaerobic conditions with error bars representing two standard deviations from the mean.

The mass loss rate profiles are shown in Figure 10 with the experimental error. Due to the extremely sharp initial peak, the graphs were split into two so the scale of the y-axis would be appropriate to the size of the mass loss rate values. The normalized error was 51, 51, and 28% at 20, 40, and 60 kW m^{-2} respectively. The error in the initial peak (shown in the inset) was not included in these numbers, as the scale of the mass loss rate and associated error was so much larger and would have given an unrealistic picture of the scatter in the data.

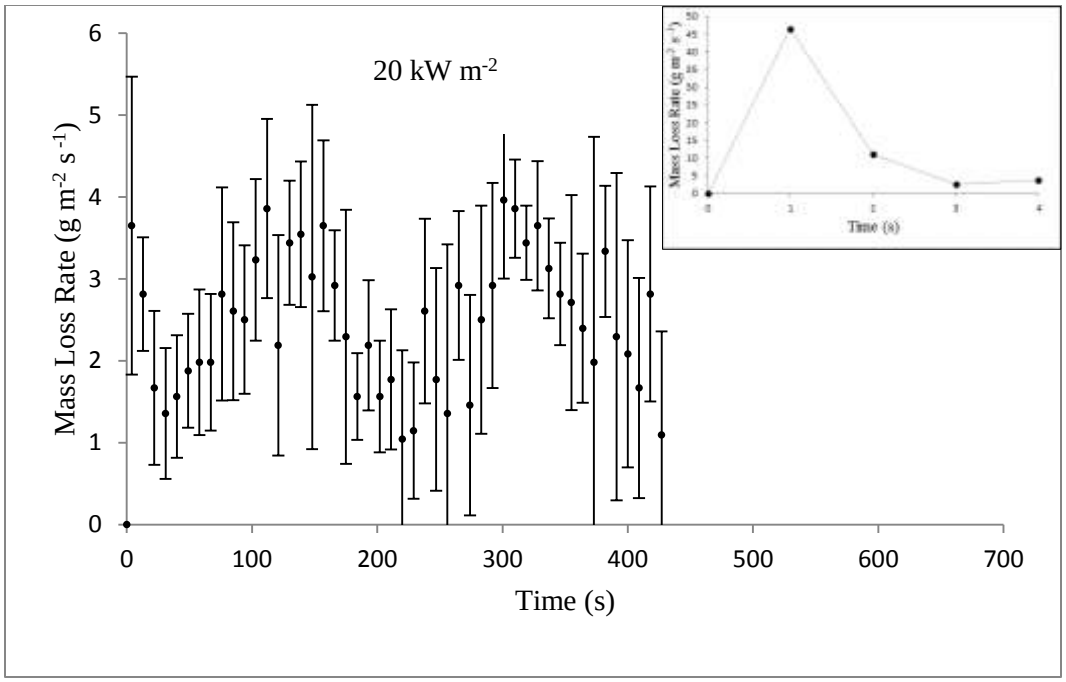
20 kW m-2
Mass Loss Rate (g m-2 s-1)
Time (s)
0
1
2
3
4
5
6
0
100
200
300
400
500
600
700

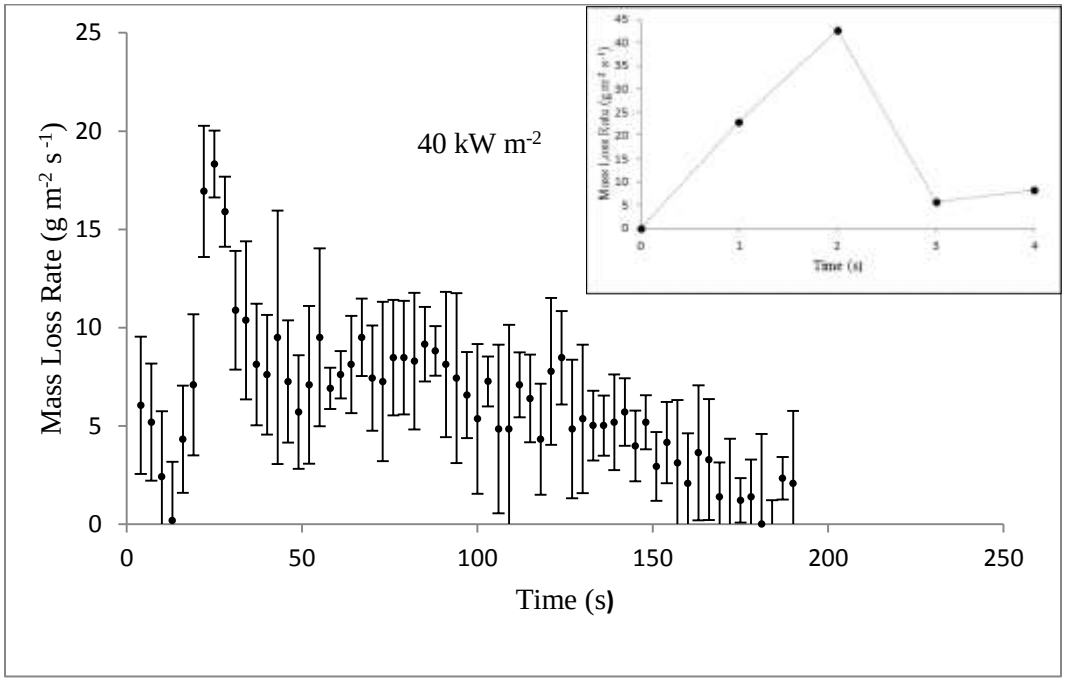
40 kW m-2
Mass Loss Rate (g m-2 s-1)
Time (s)
0
5
10
15
20
25
0
50
100
150
200
250

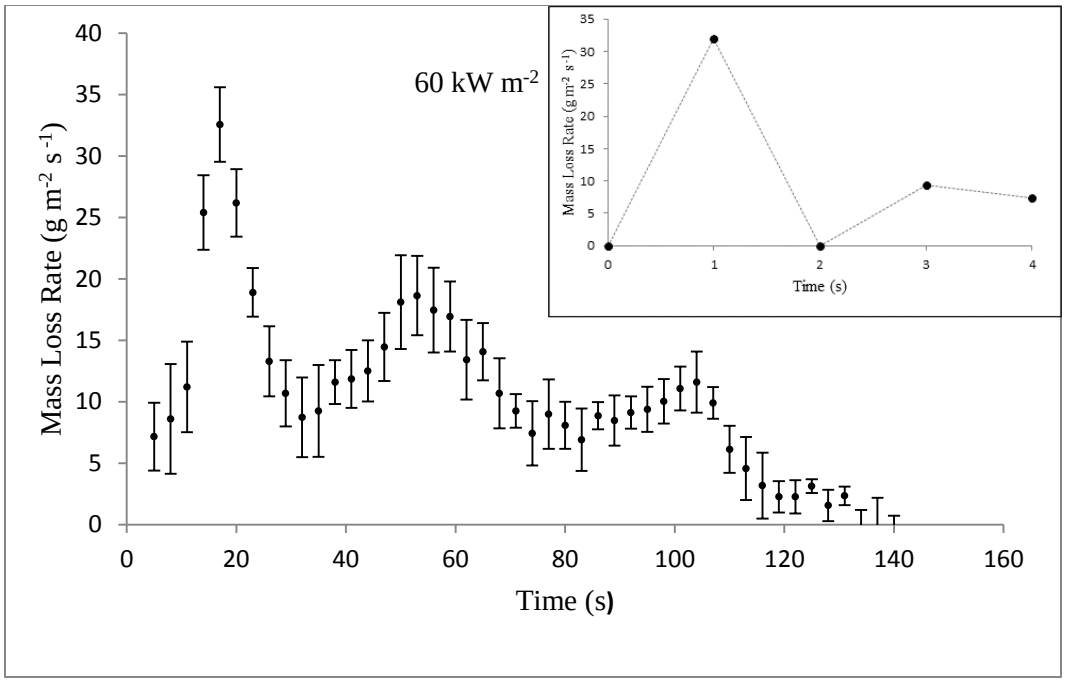

Figure 10. Mass loss rate profiles of samples with added moisture (12.6 wt.% water) collected under anaerobic conditions with error bars representing two standard deviations. The inset in the upper right-hand corner shows the first several seconds of the data where the initial moisture evaporation occurs.

4. MODEL RESULT

4.1 Non-Oxidative Pyrolysis

Tests were performed in the CAPA at 2.2 vol.% oxygen. This was the lowest achievable concentration of oxygen and was meant to simulation non-oxidative pyrolysis. Data collected from the CAPA has been validated against similar tests performed in 100 % nitrogen [5].

4.1.1 Model Development

Previous experiments were done on corrugated cardboard in air [24]. In these experiments, the sample ignited and it was assumed that the flame on top of the sample kept oxidation from occurring. This assumption broke down as the flame began dying and only partially covered the sample surface. Bench-scale tests were done in the cone calorimeter and milligram-scale tests were performed in a Thermogravimetric Analysis (TGA) system. The physical properties of the corrugated cardboard were isolated and measured during these tests.

The burning process of the cardboard was divided into four distinct sections: the virgin cardboard, the intermediary, the initial char, and the final char. The virgin cardboard (CB_a) represented the original state of the sample, the intermediary (CB_b) was an arbitrary distinction of the state between the virgin state and the initial char, the initial char ($CB_{char,1}$) and final chars ($CB_{char,2}$) represented the first and second state of the char produced during pyrolysis. The virgin char converted to the intermediary, which then converted to the initial char and further decomposed into the final char. The reactions are shown in Table 2.

Table 2. Non-oxidative reaction scheme, with the Arrhenius parameters and heats for each reaction.

	Reaction	A (sec^{-1})	E_a ($J\ mol^{-1}$)	h_r ($J\ g^{-1}$)
1	$H_2O_\ell \rightarrow H_2O_g$	6.14	2.35×10^4	-2.5×10^3
2	$CB_a \rightarrow 0.9CB_b + 0.1CB_{volatiles}$	7.95×10^9	1.3×10^5	0
3	$CB_b \rightarrow 0.37CB_{char,1} + 0.63CB_{volatiles}$	2.0×10^{11}	1.6×10^5	-1.3×10^2
4	$CB_{char,1} \rightarrow 0.59CB_{char,2} + 0.41CB_{volatiles}$	2.61×10^{-2}	1.7×10^4	0

The thermo-physical properties of all the elements in the above reactions were determined through a combination of experimental analysis, data fitting, and literature review. More information on the process used to develop this original model can be found in [12]. The final set of parameters are shown in Table 3.

Table 3. Thermo-physical properties used in the ThermaKin model.

Component	ρ ($kg\ m^{-3}$)	c ($J\ g^{-1}\ K^{-1}$)	κ ($W\ m^{-1}K^{-1}$)	ϵ
H_2O_ℓ	--	$5.2 - 6.7 \times 10^{-3}T + 1.1 \times 10^{-5}T^2$	--	--
H_2O_g	--	$2.4 - 1.6 \times 10^{-3}T + 2.0 \times 10^{-6}T^2$	--	--
LB	520	1.8	0.10	0.70
LB_{int}	470	1.55	$0.05 + 7.5 \times 10^{-11}T^3$	0.78
LB_{char1}	170	1.3	$1.5 \times 10^{-10}T^3$	0.85
LB_{char2}	100	1.3	$1.5 \times 10^{-10}T^3$	0.85
CFL	49	1.8	0.10	0.70

CFL_{int}	44	1.55	$0.05 + 7.5 \times 10^{-10} T^3$	0.78
CFL_{char1}	16	1.3	$1.5 \times 10^{-9} T^3$	0.85
CFL_{char2}	9.4	1.3	$1.5 \times 10^{-9} T^3$	0.85
BFL	74	1.8	0.10	0.70
BFL_{int}	67	1.55	$0.05 + 7.5 \times 10^{-10} T^3$	0.78
BFL_{char1}	25	1.3	$1.5 \times 10^{-9} T^3$	0.85
BFL_{char2}	15	1.3	$1.5 \times 10^{-9} T^3$	0.85
CB_{vol}	--	1.3	--	--
Kaowool PM	256	1.07	$0.052 - 4 \text{ x } 10^{-5} T + 1 \text{ x } 10^{-7} T^2$	--

The previous model was developed under flaming conditions. As described above, the flame was assumed to prevent oxidation, but this assumption broke down as the flame did not cover the whole surface towards the end of the tests. Since the experiments performed in this thesis were conducted under extremely controlled boundary conditions, it was assumed that the resulting data could be used to tweak the model to produce better results. After much iteration with the model, where parameters were varied within reasonable ranges in a systematic fashion, it was determined that the original model provided the best fit of the new data. It was possible to achieve slightly better agreement, but it required adding a level of complexity to the model that was not supported by the data.

4.1.2 Results

The temperature profiles obtained from the CAPA in 2.2 vol.% oxygen at 20, 40, and 60 kW m^{-2} are shown along with the model in Figure 11. During the pyrolysis process, the cardboard shrank slightly, the glue holding the flutes and linerboards together started to break down, and the layers curled up and flaked off. In order to minimize the exfoliation of the top layers, retaining clips were used to keep the top surface as flat as possible. Despite this, the sample still shrank and the edges of the sample curled upwards. The shrinking could have shifted the position of the thermocouples slightly. Due to the nature of cardboard pyrolysis, it was not expected that the model would accurately capture the entire temperature profile; however attention was paid to capturing the final temperatures and overall trends.

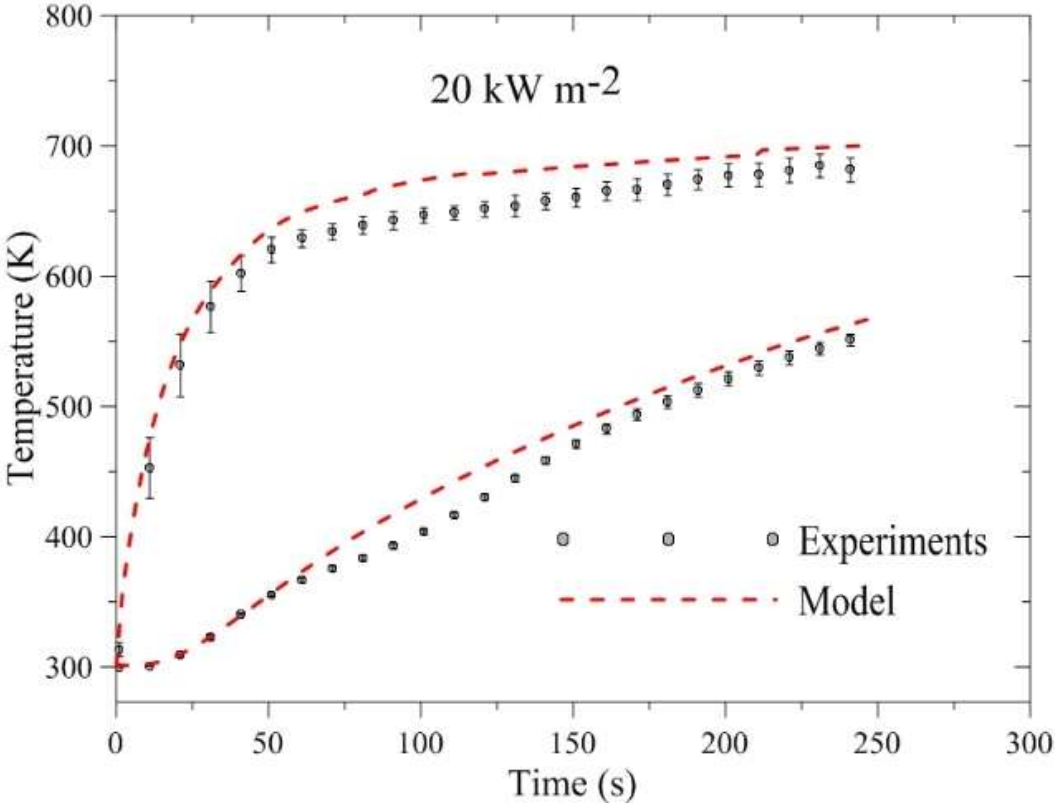
20 kW m-2
Temperature (K)
Time (s)
Experiments
Model
800
700
600
500
400
300
0
50
100
150
200
250
300

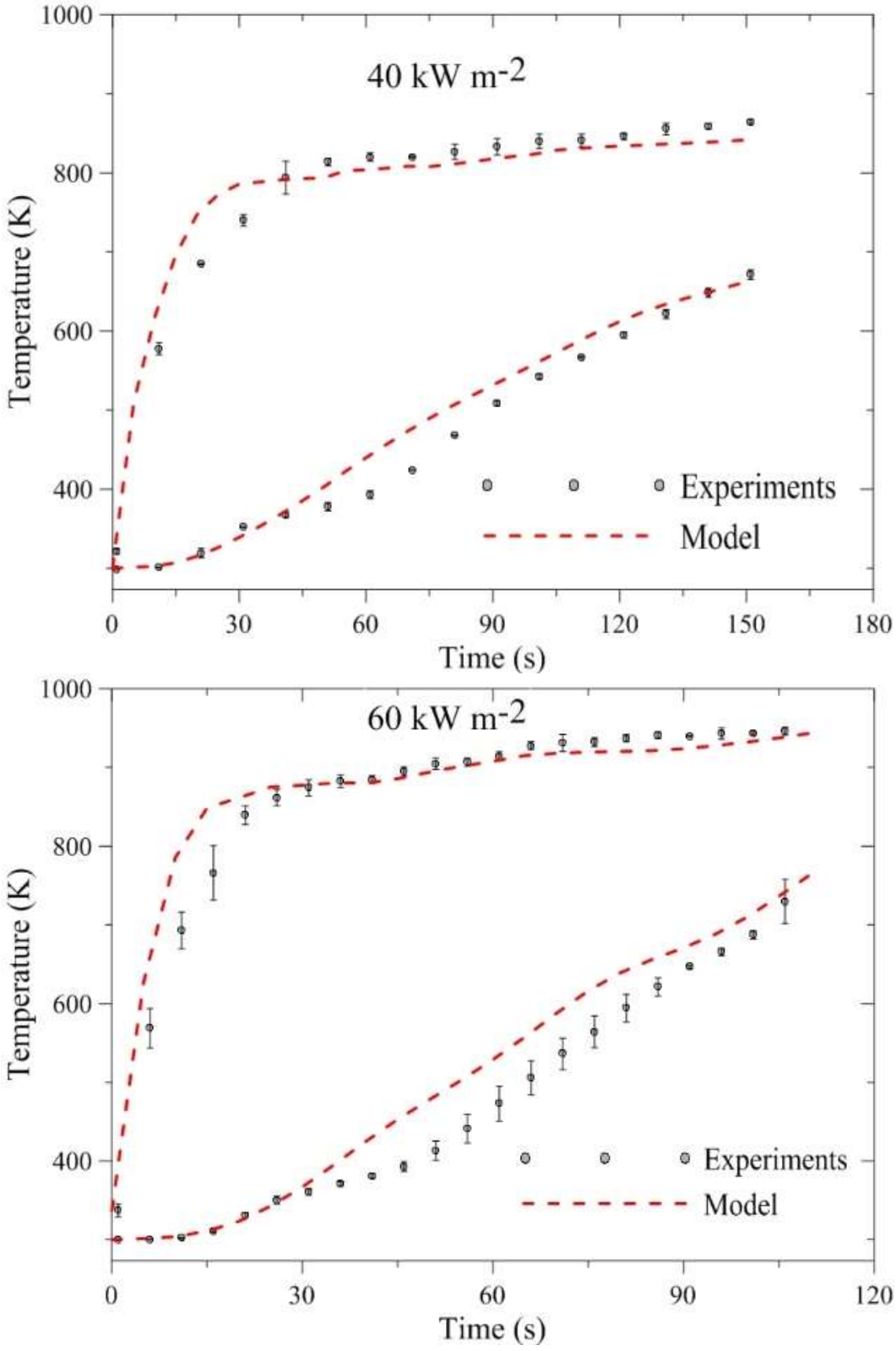

Figure 11. Non-oxidative temperature profiles with the model.

The average instantaneous discrepancy between the model and the experimental data was 3.05%, 3.95%, and 5.29% for 20, 40, and 60 kW m^{-2} respectively. These deviations were similar in magnitude to those observed in modeling of the cone calorimetry experiments based on which this parameter set was developed. In the top thermocouple, the initial temperature rise accounted for most of this error for the higher heat fluxes, as the model over-predicted this period by 10.3% for 40 kW m-2 and 12.9% for 60 kW m^{-2}. For the bottom thermocouple, the temperature was slightly over-predicted by 2.8%, 4.48%, and 7.1% respectively. As was stated above, this error is most likely attributed to the shrinking and peeling that the sample experienced during the pyrolysis process.

As described in previous sections, the temperature data was used to fit the ThermaKin model. The mass loss rate profiles were used as a validation that the model was accurately capturing the cardboard pyrolysis. The mass loss rate profiles obtained in the CAPA at 2.2 vol.% oxygen are shown with the calculated model at 20, 40, and 60 kW m^{-2} in Figure 12. There are some discrepancies between the mass loss rate data and the model. Due to the complicated nature of cardboard pyrolysis, it was not expected that all aspects of the mass loss rate profiles would be accurately predicted. The shrinking and exfoliation experienced by the sample would ostensibly affect the mass of the sample. In addition, as the sample shrank, radiation was allowed to heat the sample from the sides as well as the top of the sample and the one-dimension assumption that the model was based on breaks down. The thermocouples were placed near enough to the center of the sample that they did not feel this extra radiation, and thus the data set is still valid for fitting the model. Therefore, we were able to accurately model the temperature profiles but cannot represent all aspects of the mass loss rate plot.

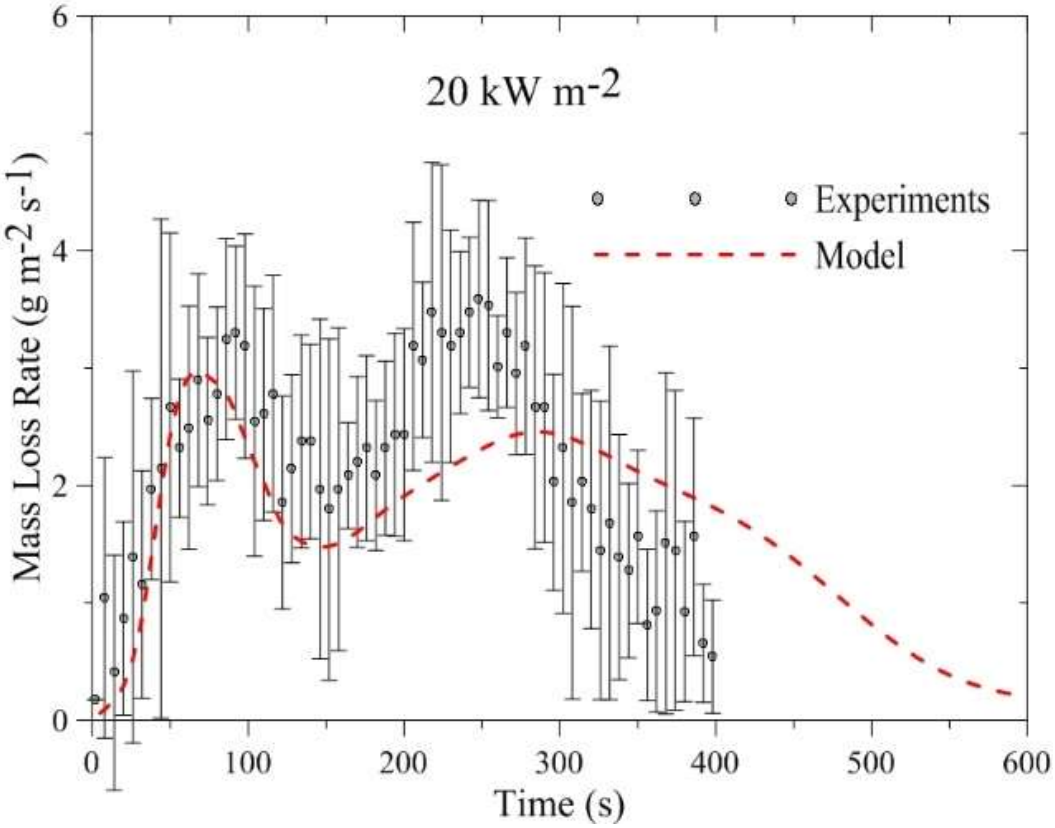
20 kW m-2
Experiments
Model
Mass Loss Rate (g m-2 s-1)
Time (s)
0
2
4
6
0
100
200
300
400
500
600

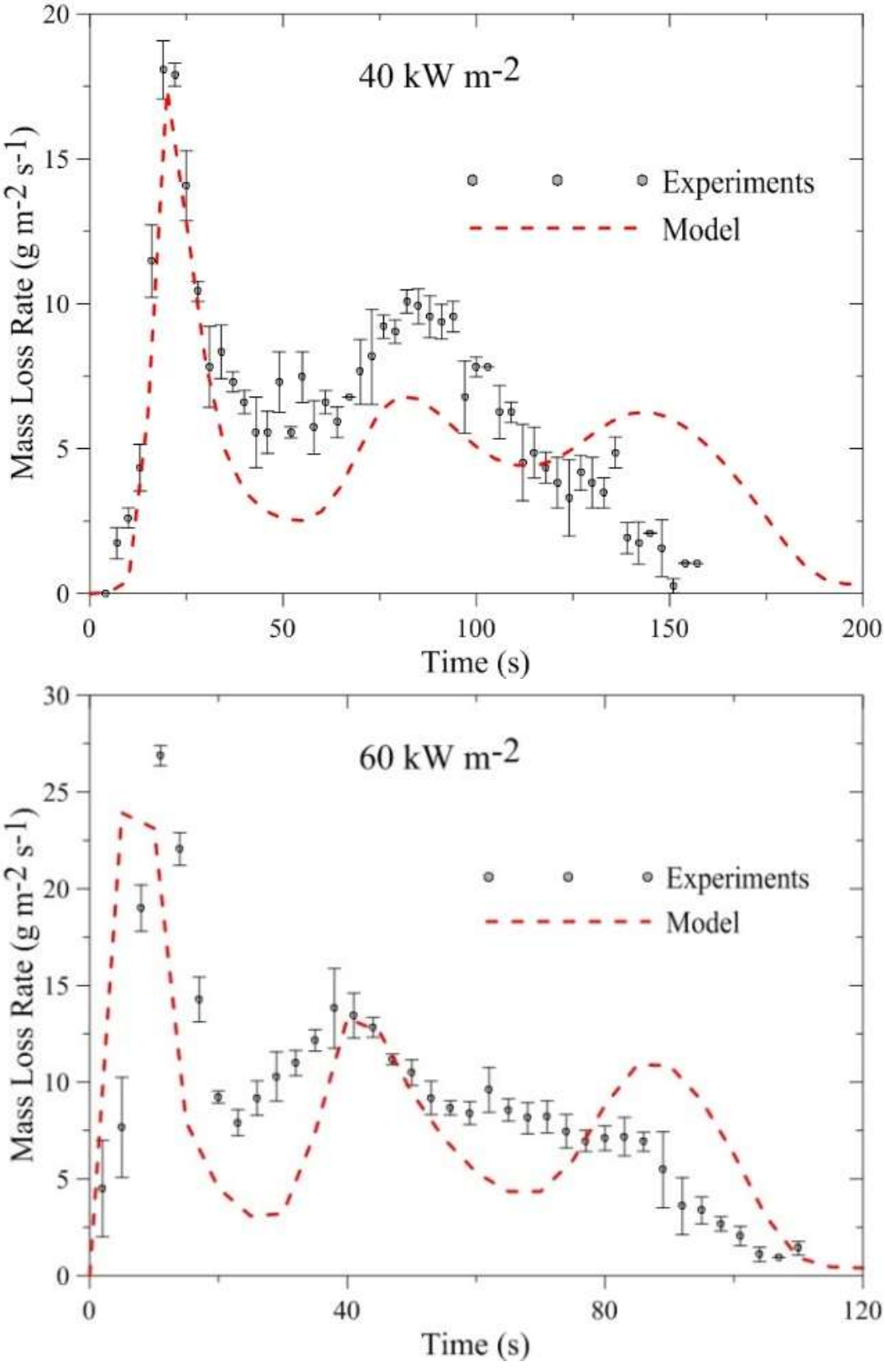

Figure 12. Non-oxidative mass loss rate profiles with the model.

The mass loss rate profile of the 60 kW m^{-2} was quite well predicted by the model, as were the first peaks of the mass loss rate curves predicted for 20 and 40 kW m^{-2}. The total burning time of the 20 and 40 kW m^{-2} profiles are over-predicted by the model by 197 and 67 seconds respectively. The peak of 20 kW m^{-2} was under-predicted by 9.2%. The 40 kW m^{-2} test was predicted almost exactly, while the highest heat flux was under-predicted by 13.9%.

Another way to view the total mass loss is through the final char yield. The mass loss rate data was used to find the percentage of the original mass that remained at the end of each test. The non-oxidative experiments had an average char yield of 37.3%, 27.9%, and 26.8% for 20, 40, and 60 kW m^{-2} respectively, while the previously conducted tests which had the flame on the surface resulted in final char yields of 17.8%, 16.7%, and 14.2% respectively. A comparison of the two experiments shows that the char yields were higher in the non-oxidative tests, indicating that oxygen reacted with the corrugated cardboard char during the flaming tests to increase the total mass lost.

4.1.3. Uncertainty

An analysis was done when developing the previous model on the uncertainty in the model parameters. The uncertainties in the TGA-fitted reaction kinetics are approximately ± 50% for the pre-exponential factors, ± 3% for the activation energies and ± 5% for the stoichiometric coefficients. The uncertainties in the cardboard component densities were assumed to be the same as those of the virgin cardboard components, ± 10%, as derived from geometric measurements. The uncertainties in the thermal conductivity and emissivity values were approximately ± 15%.

The heats of the decomposition reactions and cardboard component heat capacities carried the most significant uncertainties of ± 20%. These uncertainties are a result of poor repeatability in the DSC measurements. The uncertainty in the PCFC-measured total effective heat of combustion was, according to the standard [16], ± 6%.

4.2 Oxidative Pyrolysis

Tests were performed in 10.5 vol.% oxygen in the CAPA. This concentration of oxygen represents the highest concentration at which the cardboard sample will not ignite at 60 kW m^{-2}. The purpose of these experiments was to examine the effects of oxidation without the uncertainty introduced by the presence of a flame. The temperature profiles of the anaerobic and oxidative environments are shown in Figure 13.

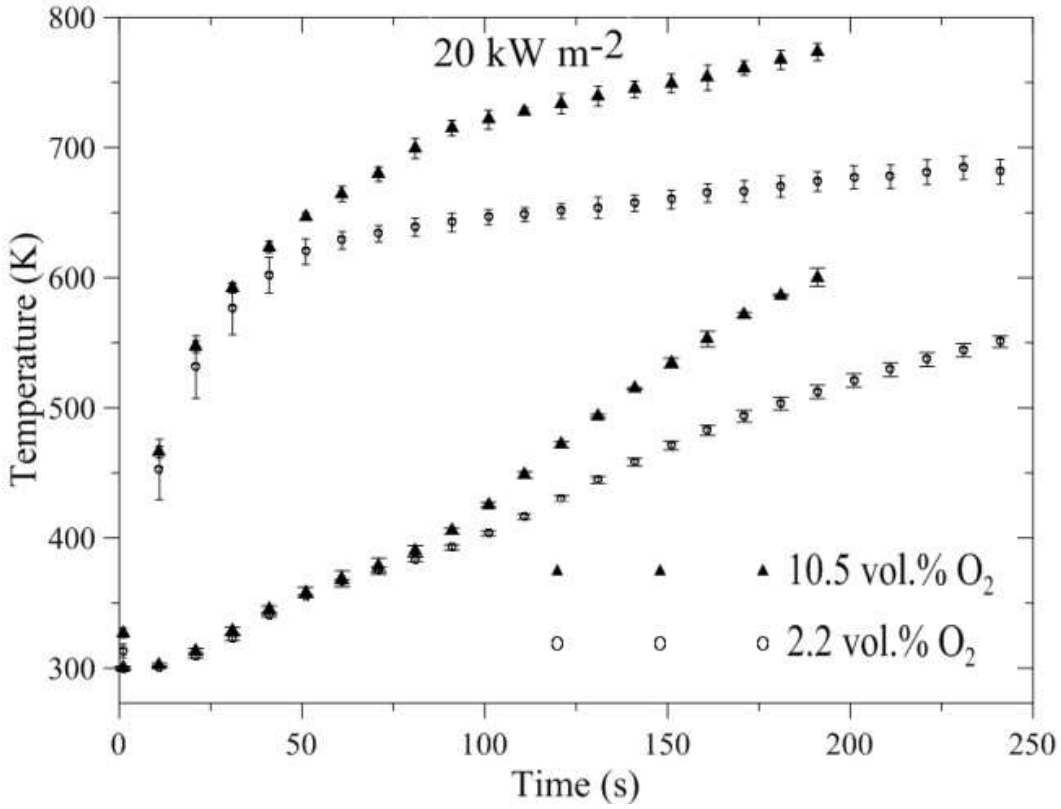

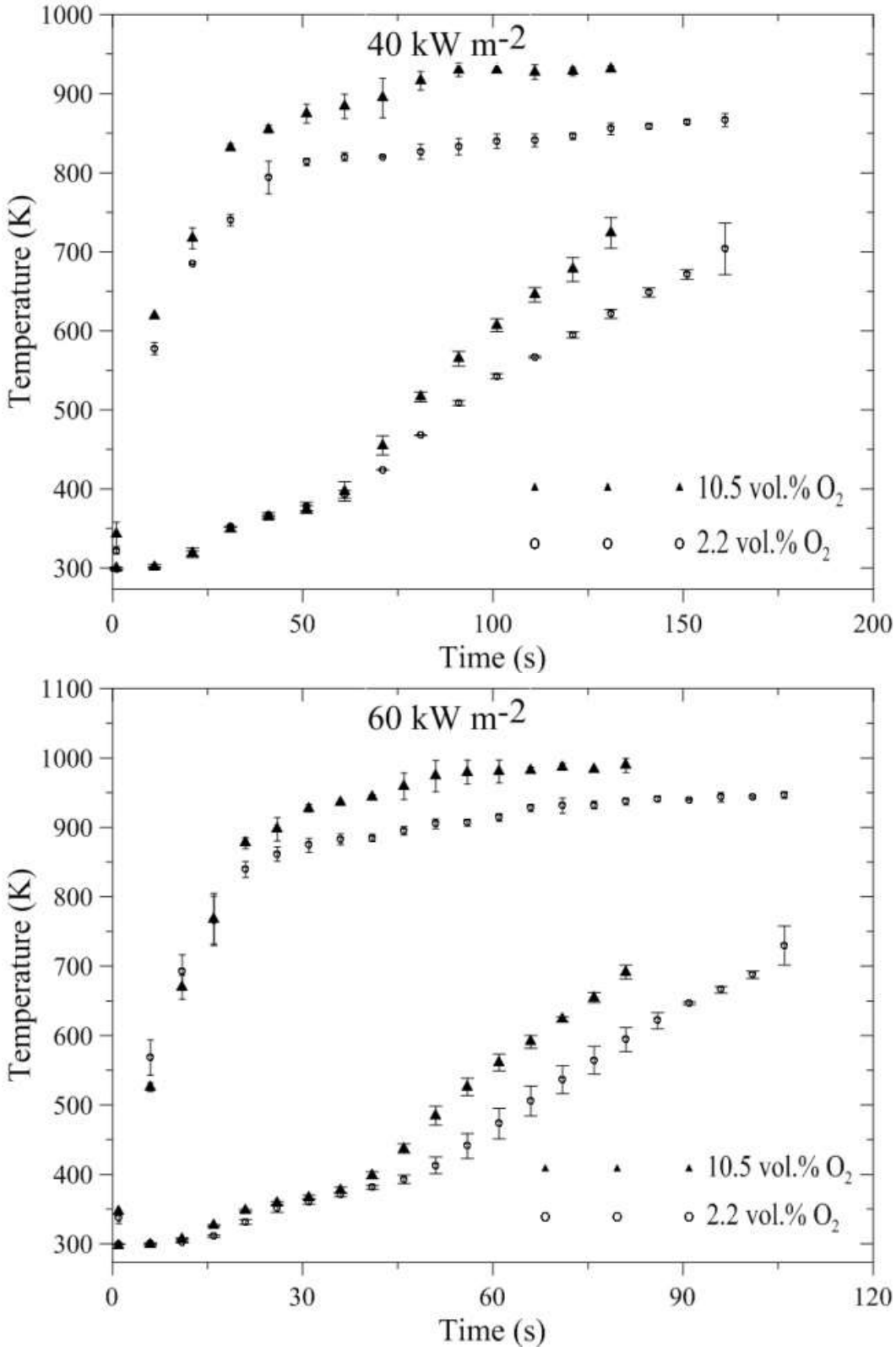

Figure 13. A comparison of the temperature profiles collected under oxidative and non-oxidative conditions.

It is evident that the presence of additional oxygen in the pyrolysis atmosphere had a definite effect on the temperature profiles and burning kinetics of the sample. The temperature profiles of the anaerobic and oxidative pyrolysis are very similar up to a certain threshold temperature. After that point, the oxidative pyrolysis temperatures became much higher than the anaerobic pyrolysis temperatures. This is consistent with the temperature behavior exhibited by other cellulosic materials as discussed in the introduction. The oxidative temperature profiles were consistently higher than the anaerobic pyrolysis temperature profiles, but this difference diminished as the heat flux increased. This is consistent with the research presented in the introduction, in which it was pointed out that char production was initially encouraged by the increased presence of oxygen. However, at higher heat fluxes the production of char already occurred rapidly due to the extreme heat imposed on the sample, and the differences in the production of char is less noticeable. This effect was also noticed in the mass loss rate profiles. The anaerobic and oxidative mass loss rate profiles at each heat flux are shown together in Figure 14.

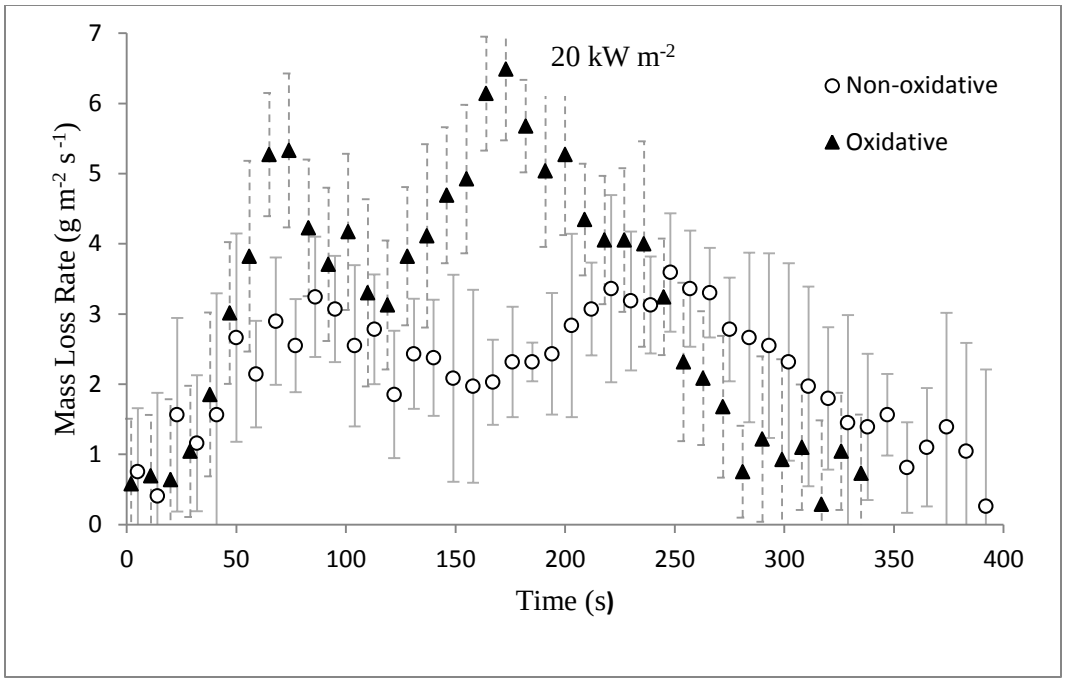
20 kW m-2
Non-oxidative
Oxidative
Mass Loss Rate (g m-2 s-1)
Time (s)
0
1
2
3
4
5
6
7
0
50
100
150
200
250
300
350
400

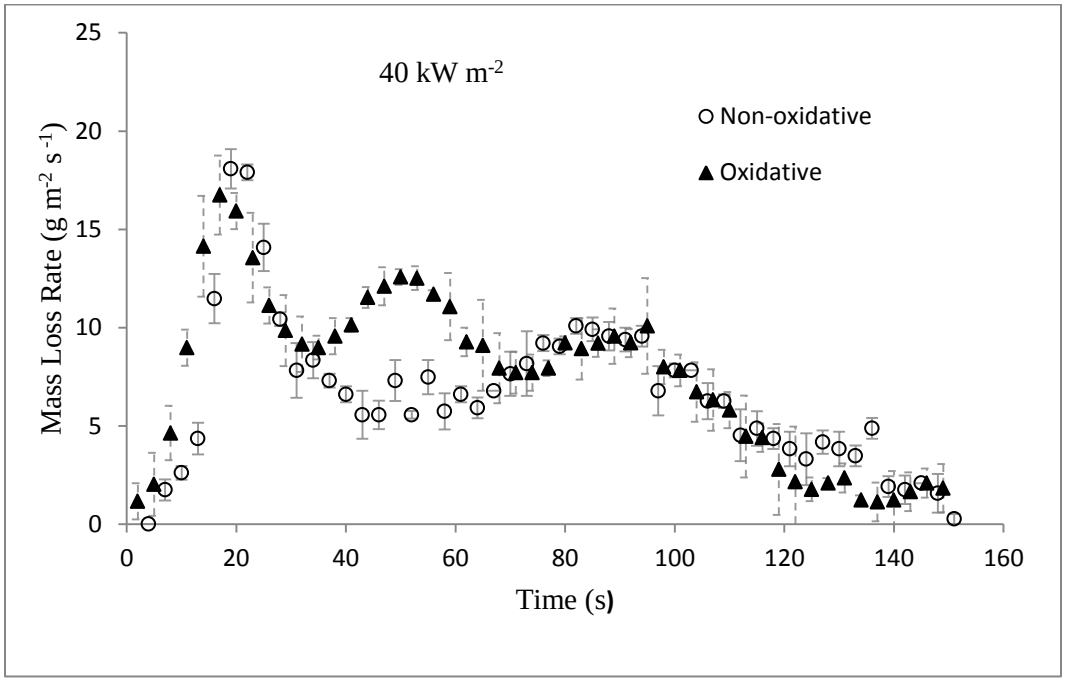
40 kW m-2
Non-oxidative
Oxidative
Mass Loss Rate (g m-2 s-1)
Time (s)
0
5
10
15
20
25
0
20
40
60
80
100
120
140
160

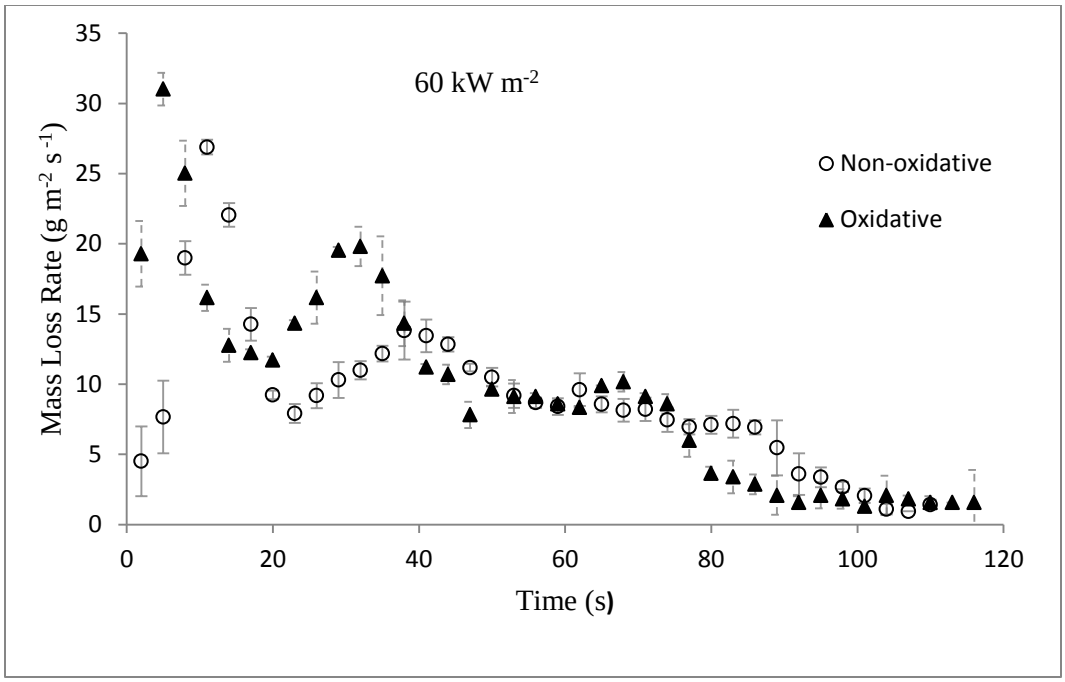

Figure 14. A comparison of the mass loss profiles of non-oxidative and oxidative pyrolysis.

The addition of oxygen to the gas atmosphere increased the first and second peak of the mass loss rate profiles. This was most evident at 20 kW m^{-2}. The average mass loss rate increased across the board as well with the addition of oxygen. The average mass loss rate for the anaerobic pyrolysis was 2.2, 6.4, and 8.6 g m^{-2} s^{-1} at 20, 40, and 60 kW m^{-2} respectively. For the oxidative pyrolysis, the average mass loss rate was 3.2, 7.4, and 9.6 g m^{-2} s^{-1} at 20, 40, and 60 kW m^{-2} respectively. The difference between the average mass loss rates decreased from 46.5% to 16.5% to 12.7% as the heat flux increased, mirroring the behavior seen in the temperature profiles above.

It is possible to visually see the differences between the non-oxidative and oxidative gasification tests. In Figure 15, the samples after tests at 40 kW m^{-2} are shown. In the non-oxidative test, the sample was smoother and showed less exfoliation. The sample

also shrunk less. The oxidized sample has turned white around the edges, which shows the development of ash, and has peeled up and flaked away in some places.

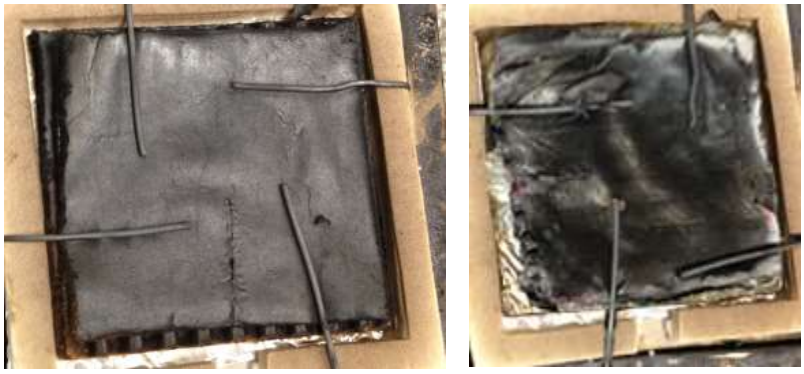

Figure 15. Samples after being gasified under 40 kW m-2 in non-oxidative (left) and oxidative (right) conditions.

4.2.1 Kinetics of Oxidation

The presence of oxygen changed the reaction mechanism. The reaction mechanisms used in the non-oxidative model were developed by fitting normalized mass and mass loss rate data taken in the TGA at 100 % nitrogen with four reactions [24]. In order to develop a set of oxidation reactions, data was collected in the TGA at 10 and 21 vol.% oxygen. The normalized mass and mass loss rate data measured were fitted with a universal reaction mechanism that included oxidation reactions. The resulting reaction mechanism is shown in the introduction in Table 1. It was possible to achieve a slightly better fit of the data, but this set of reactions provided a good fit while maintaining a level of simplicity. It should be noted that the reactions shown in Table 1 represent the original model developed, and these reactions and parameters were modified in the next section based on the oxidative data collected in the CAPA.

Oxidation reactions were added to the third and fourth reactions of the non-oxidative mechanism. The first two oxidation reactions (3a and 3b) occur in parallel with the second anaerobic decomposition reaction (3) to convert the intermediary into the initial char. The third reaction (4a) occurs in parallel with the third anaerobic decomposition reaction (4). The fourth oxidation reaction (5) converts the final char into ash. The definition of this new component in the model is discussed in the following section.

4.2.2 Model Development

The previous model was developed under the assumption that no oxidation occurred. In the scenario described in the previous section, oxidation clearly has occurred, and the model had to be modified to incorporate the oxidation reaction mechanism developed using the previous TGA data. In the new model, the elements of the previously developed anaerobic model were left untouched, while ash was added as a component. Three different components were created; one representing the ash formed from the liner board, and two representing the ash from the two flute layers. Since the value for the heat capacity of the liner board ash was found to be very close to the value for the final char of the flutes, it was assumed that these components had the same density. The density of the ash of the flutes was scaled in the same ratio as the final chars of the flute. The thermal conductivity of the liner board and flute ash was assumed to be the same as the final char thermal conductivity for each respective component. The inputs into the model are shown in Table 4.

Table 4. The additional thermo-physical properties needed for the oxidative model.

Component	ρ (kg m^{-3})	c (J g^{-1} K^{-1})	κ (W m^{-1}K^{-1})	ϵ
O_2	--	$.827 - 0.35 \times 10^{-3}\, T - 8.9 \times 10^{-2} T^2$	--	--
LB_{ash}	15.3	1.3	$1.5 \times 10^{-10} T^3$	0.85
CFL_{ash}	1.41	1.3	$1.5 \times 10^{-9} T^3$	0.85
BFL_{ash}	2.22	1.3	$1.5 \times 10^{-9} T^3$	0.85

The original assumption when adjusting the model was that the specified concentration of oxygen was evenly distributed throughout the sample. It was also initially assumed that the added oxidation reactions were thermally neutral. After some iteration with the model, it was apparent that the oxidation of the char had to be generating some heat to predict the temperature profiles accurately. There are four oxidation reactions; two occur in parallel to convert the intermediary to the initial char, and two occur sequentially to convert the initial char to the final char and the final char to ash. The comparison of the anaerobic model with the oxidative data shows that the differences do not get severe until approximately 700 K. At this point, the anaerobic model clearly falls outside the range of the oxidative data. The TGA data indicates that the first two oxidation reactions that occur in parallel happen before this temperature, so it was assumed that these reactions were thermally neutral. The heats on the last two oxidation reactions were scaled so that each reaction was producing the same amount of heat per unit mass pyrolyzed in the reaction. After iteration with the model, the last reaction was fitted with a heat of 2.04 x 10^7 and the previous reaction was fitted with 1.25 x 10^7. These reactions correspond with reactions 4a and 4b in Table 4.

After adding heat to the last two oxidation reactions, it became clear that diffusion of oxygen throughout the sample was a limiting factor since it was not possible to predict the top linerboard temperature without severely over predicting the bottom linerboard temperature. The diffusion of oxygen from the top surface through the sample was introduced into the model.

When developing this new model, the Arrhenius coefficients had to be modified. When these parameters were first developed for the original model, they were fitted from TGA data and the presence of oxygen was accounted for in these values. Since the model being developed for oxidation specifically adds oxygen as a component, the effects of oxidation was to be taken out of the Arrhenius pre-exponential factor by dividing the original values by the mass concentration of oxygen at the surface. The stoichiometric coefficients of the oxygen in the reaction were assumed to be the heat of reaction divided by the universal value for the heat released during combustion per unit mass of oxygen, which has a value of 13.1 $kJ/g_{O2.}$

The values for the pre-exponential factor and the activation energy were scaled down for the last oxidation reaction in order to provide the same fit of the TGA data. The high exponent of the pre-exponential factor was causing numeric of the model to diverge, so lowering the exponent allowed the model to run through each simulation. The pre-exponential factor is 1.2×10^{80} and the new activation energy is 1.08×10^{6}. The final set of reaction parameters for 10.5 vol.% oxygen is shown in Table 5.

Table 5. Oxidative reaction scheme for corrugated cardboard with the Arrhenius pairs and heats for each reaction.

#	Reaction Equation	A (sec^{-1})	E_a ($J\ mol^{-1}$)	h_r ($J\ g^{-1}$)
1	$H_2O_\ell \rightarrow H_2O_g$	6.14	$2.35x10^4$	$-2.5x10^3$
2	$CB_a \rightarrow 0.9CB_b + 0.1CB_{volatiles}$	$7.95x10^9$	$1.3x10^5$	0
3	$CB_b \rightarrow 0.37CB_{char,1} + 0.63CB_{volatiles}$	$2.0x10^{11}$	$1.6x10^5$	$-1.3x10^2$
3a	$CB_b + 0O_2 \rightarrow 0.59CB_{char,1} + 0.41CB_{volatiles}$	$7.1x10^{10}[O_2]$	$1.6x10^5$	0
3b	$CB_b + 0O_2 \rightarrow 0.48CB_{char,1} + 0.52CB_{volatiles}$	$1.6x10^{22}[O_2]$	$2.8x10^5$	0
4	$CB_{char,1} \rightarrow 0.59CB_{char,2} + 0.41CB_{volatiles}$	$2.61x10^{-2}$	$1.7x10^4$	0
4a	$CB_{char,1} + .95O_2 \rightarrow 0.48CB_{char,2} + 1.47CB_{volatiles}$	$1.7x10^{-3}[O_2]$	$1.7x10^4$	$1.25x10^4$
5	$CB_{char,2} + 1.56O_2 \rightarrow 0.15\ ash + 2.41CB_{volatiles}$	$1.1x10^{79}[O_2]$	$1.08x10^6$	$2.04x10^4$

4.2.3 Results

The temperature profiles with the calculated ThermaKin model are shown in Figure 16. The top and bottom linerboard temperature profiles for the 20 kW m^{-2} test were both under- predicted. The average instantaneous error for the top linerboard was 4% and for the bottom was 3%. The temperature of the top linerboard collected in tests conducted at heat fluxes of 40 and 60 kW m^{-2} was slightly under-predicted by an average instantaneous error of 6% and 7%, respectively. The instantaneous error was calculated by dividing the difference between the experimental data and the model prediction by the experimental error at each data point. While the temperature of the top linerboard was quite well predicted, the bottom temperature was over predicted during the middle

portion of the tests conducted at heat fluxes of 40 and 60 kW m^{-2}. The average instantaneous error is 12% and 18%, respectively, with the majority of this error occurring between 30 and 130 seconds for 40 kW m^{-2} and between 20 and 85 seconds for 60 kW m^{-2}.

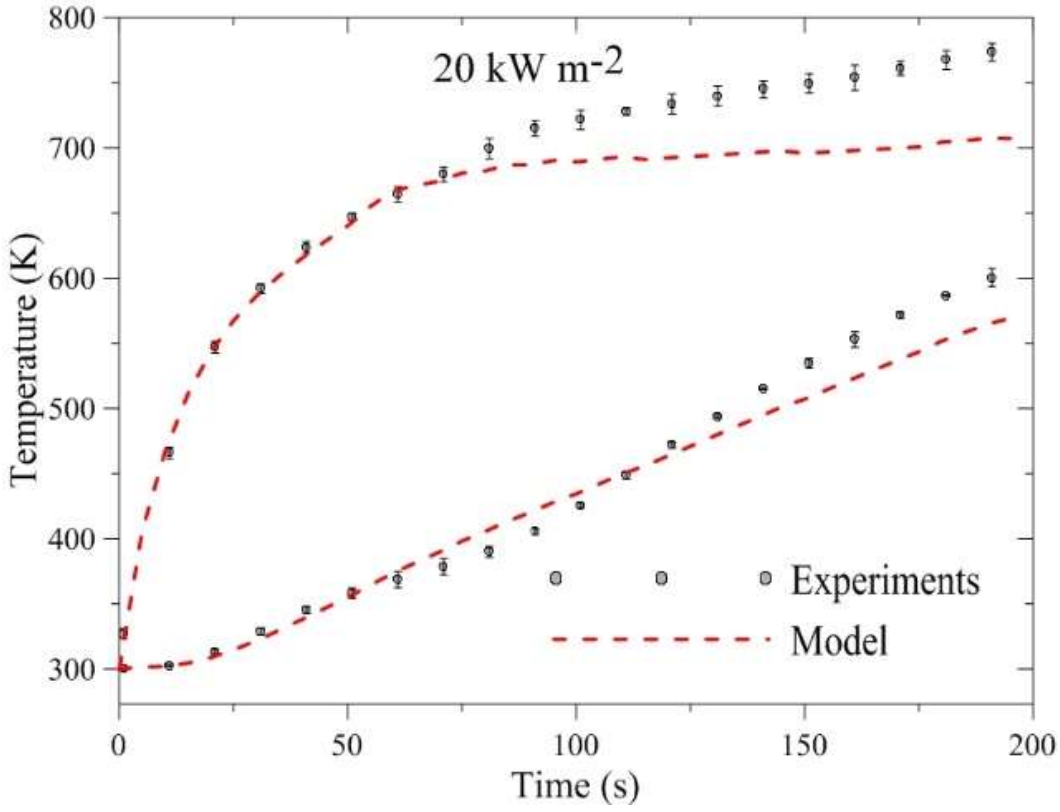

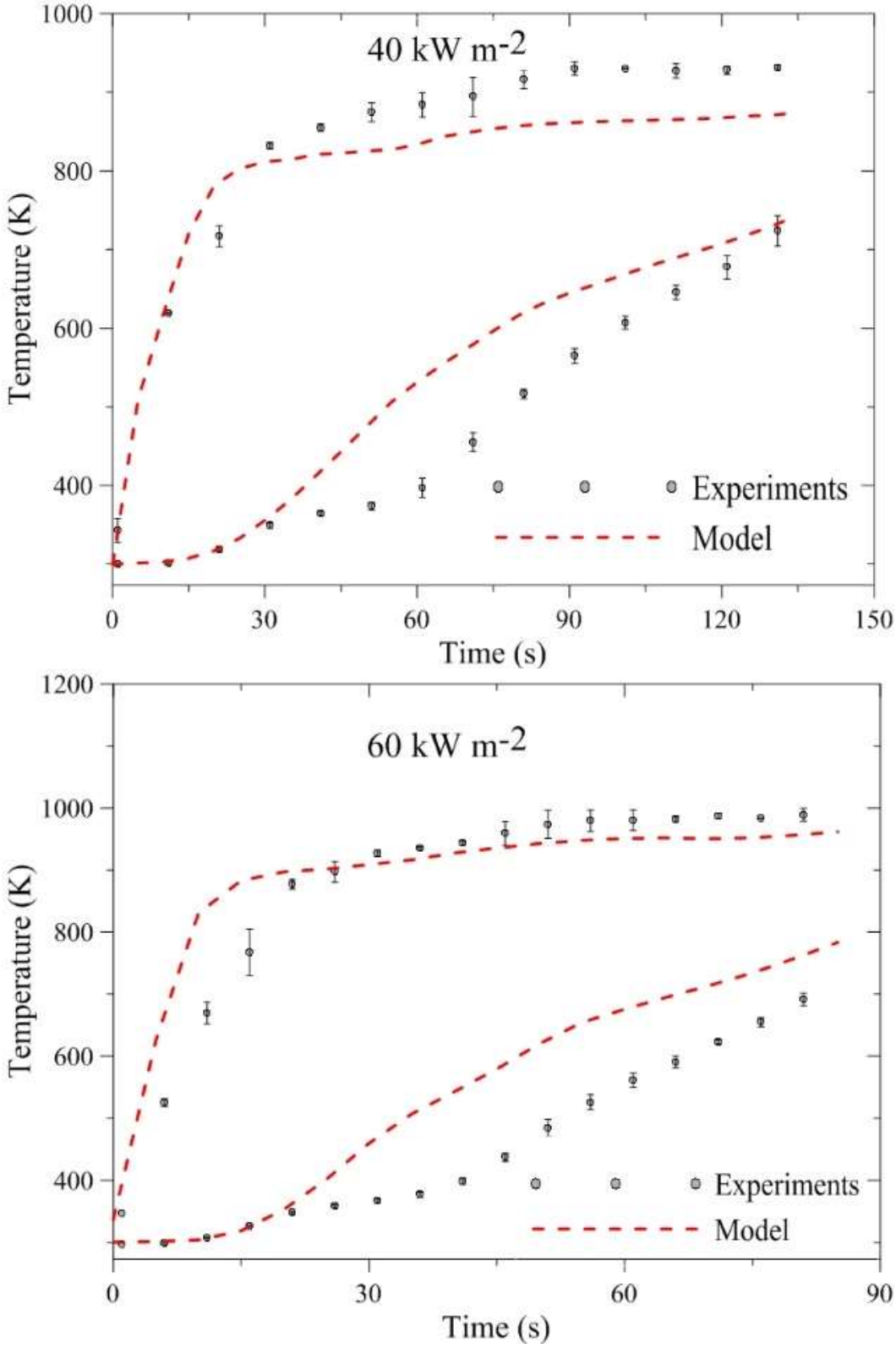

Figure 16. The oxidative temperature profiles with the ThermaKin model.

As with the non-oxidative model developed in the previous section, the one-dimensional assumption broke down as the sample shrank and the sample received radiation from the top as well as the sides. The addition of oxygen to the atmosphere led to the production of ash, which has a very low density. Some of the ash on the top layer was observed to flake off and blow away during the test. This phenomenon affected the mass loss rate data collected to validate the model. The mass loss rate profiles are shown in Figure 17.

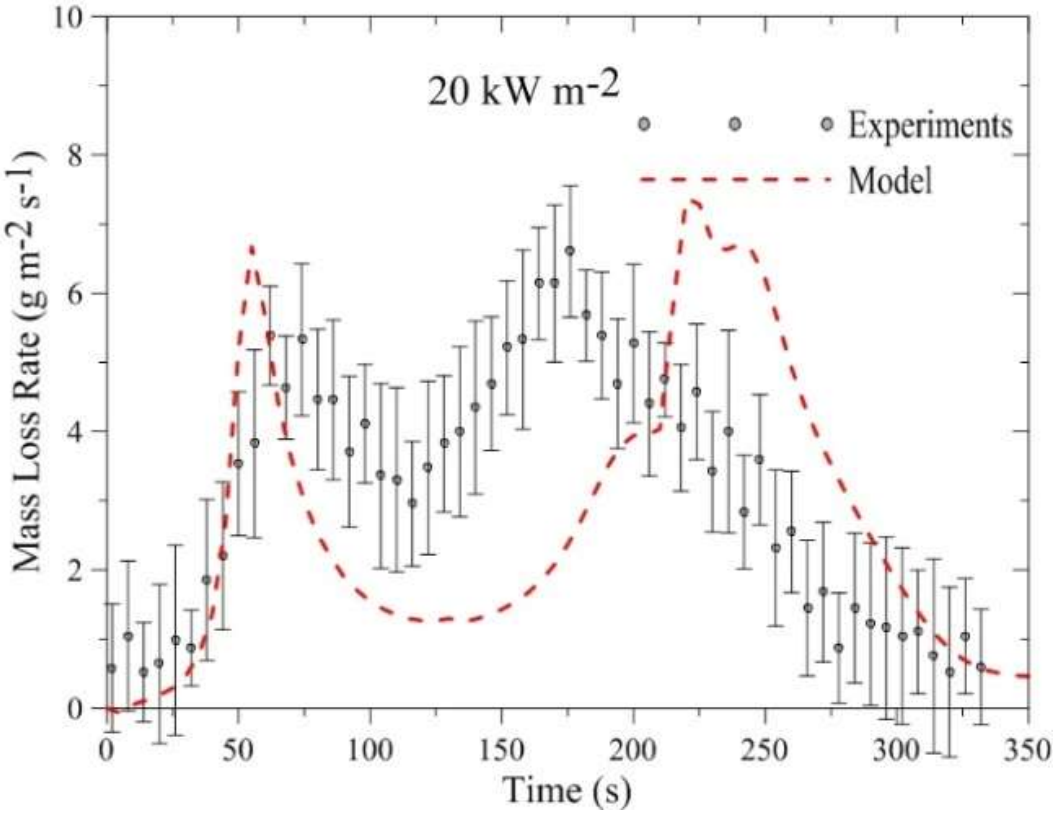

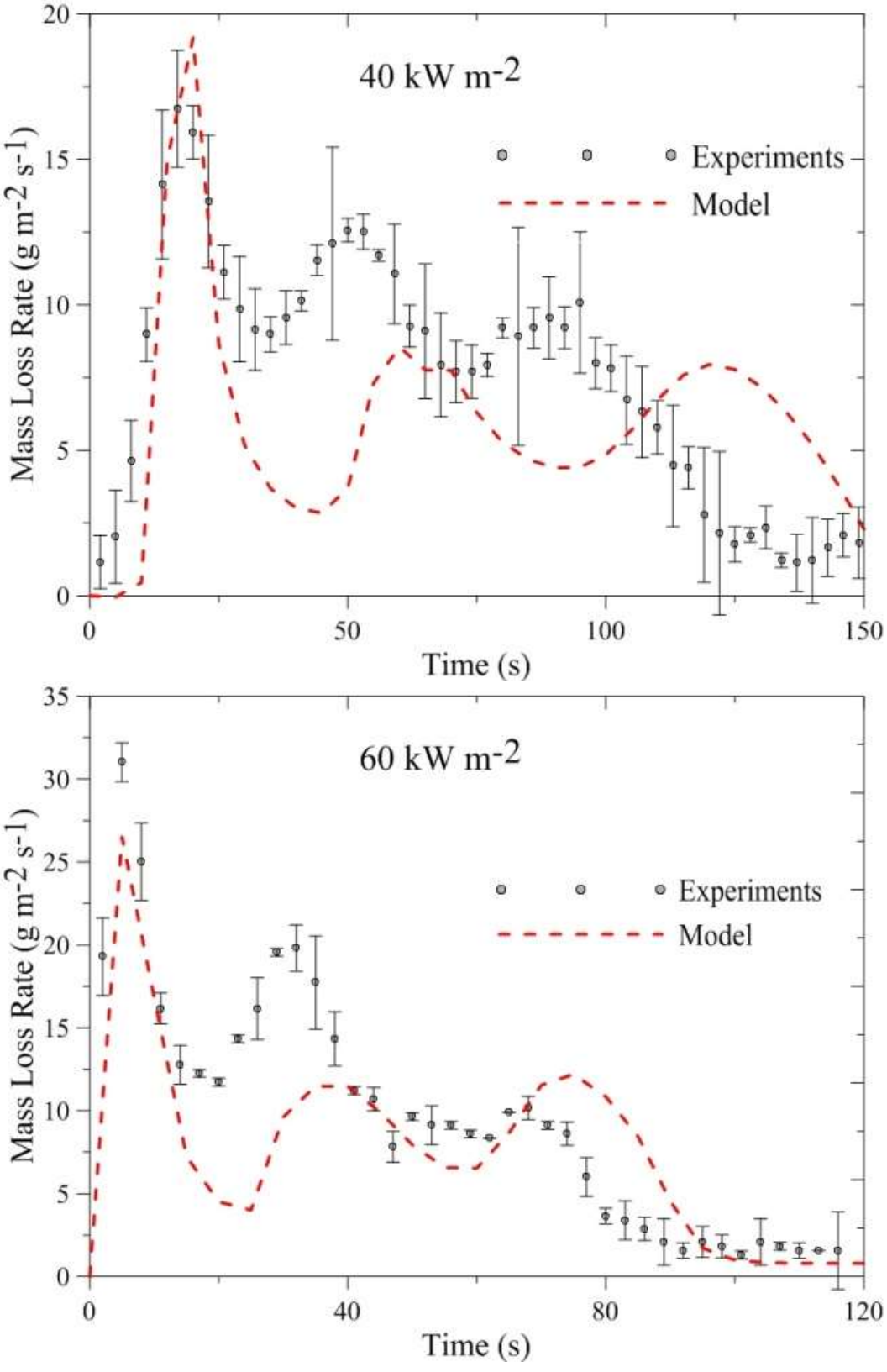

Figure 17. The oxidative mass loss rate profiles with the ThermaKin model.

The mass loss rate profiles at all heat fluxes were well predicted by the model. As with the non-oxidative model, the first peak was well modeled. The height of this first peak was predicted to within 24%, 20%, and 9%. In this case, the time offset between the prediction and the observed time of the first peak in the 20 and 60 kW m^{-2} data sets have been reduced from the non-oxidative case. The total burning time and the initial rise and magnitude of the first peak were all predicted well by the oxidative model. The second peaks were not well predicted by the model. As was stated in the previous section on the non-oxidative model, it was expected that the model would not accurately predict these sections due to the burning nature of the corrugated cardboard sample.

Another indication of the quality of the model is the total mass lost during the pyrolysis process. The agreement between the experimental data and model predictions can be calculated. The oxidation model predicted the total mass lost within 16%, 19%, and 20% respectively for the 20, 40, and 60 kW m^{-2} tests. This agreement indicated that the model is capable of predicting the general kinetics of the pyrolysis process even if the mass loss rate profiles were not perfectly predicted.

In the anaerobic model, it was assumed that no oxidation occurred, even though a small amount of oxygen (2.2 vol.%) was present at the sample surface. The oxidation model was modified to change the oxygen level from 10.5% to 2.2% oxygen at the surface, by volume. It was thought that this might be a more accurate representation of what was actually occurring and would perhaps make the mass loss rate profiles fit better. It was found that adding in oxidation as a component of the anaerobic model worsened the temperature model fit of the data. The addition of oxidation at the sample surface did indeed improve the mass loss rate model slightly, by increasing the height of the peaks

and shortening the overall burn time. However, since the temperature profiles were used to fit the model, oxidation was not included into the anaerobic model. The 2.2% oxygen at the sample surface was an average value, and in some regions the concentration dropped lower than that value. It is possible that the concentration of oxygen was too low to produce much of an oxidation effect, or that other factors were limiting this effect.

4.2.4 Uncertainty

The heat of reaction for the last two oxidation reactions are new parameters added to the oxidation model. Understanding the uncertainty in this parameter and the effect it has on the model is important. In Figure 18, the temperature profile at 40 kW m^{-2} is shown with two lines representing the model with a 10% increase and decrease in the heats of reaction for the last two reactions.

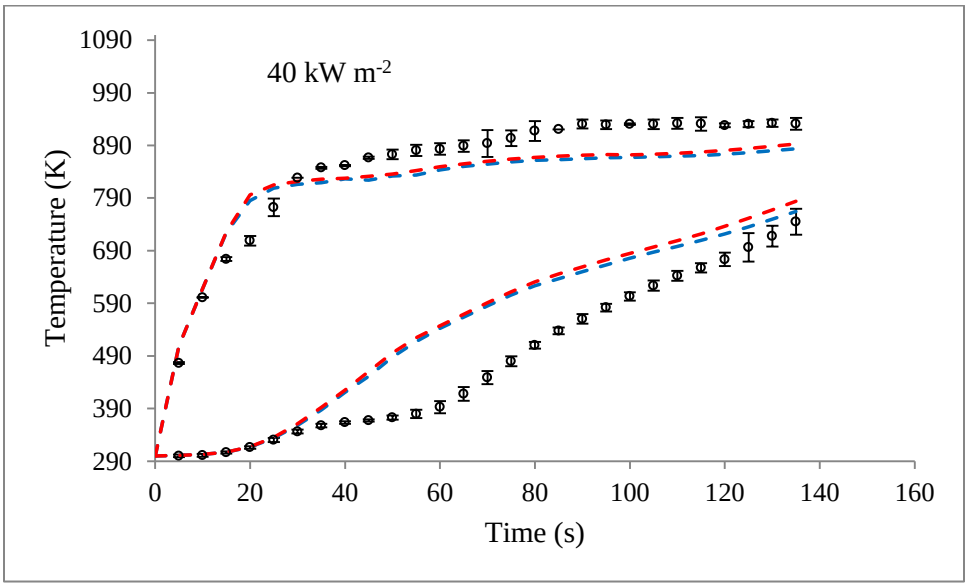

Figure 18. Temperature profile at 40 kW m-2 with two different versions of the model: one with the heats of reaction on the final two oxidation reactions increased by 10%, and the other with the heats of reaction decreased by 10%.

From the plot, it is clear that the changes in the heat of reactions have little impact on the model. The maximum difference between the model lines occurs at the end of the

simulation in the bottom linerboard, and is less than 1%, indicating that the uncertainty in the heats of reaction is very high.

4.3 Moisture Content

Tests were performed under anaerobic conditions where moisture was added to the samples to determine the effect of added water on the temperature and mass loss rate profiles. Uniform conditioning sessions produced samples with a moisture content of 12.6 ±.6 wt.%. These samples were gasified in the same manner described in the experimental section under anaerobic conditions. The temperature profiles are compared to the anaerobic data in Figure 19. The temperature profiles of the conditioned samples were not dramatically different from the standard, dried samples. The top linerboard temperatures were nearly identical. The bottom linerboard temperatures were very similar up to a threshold temperature of approximately 350 K. After that point, the temperature of the moisturized samples dipped lower than the dried samples. This dip reached a maximum of approximately 100 ºC below the anaerobic temperature profile at all heat fluxes.

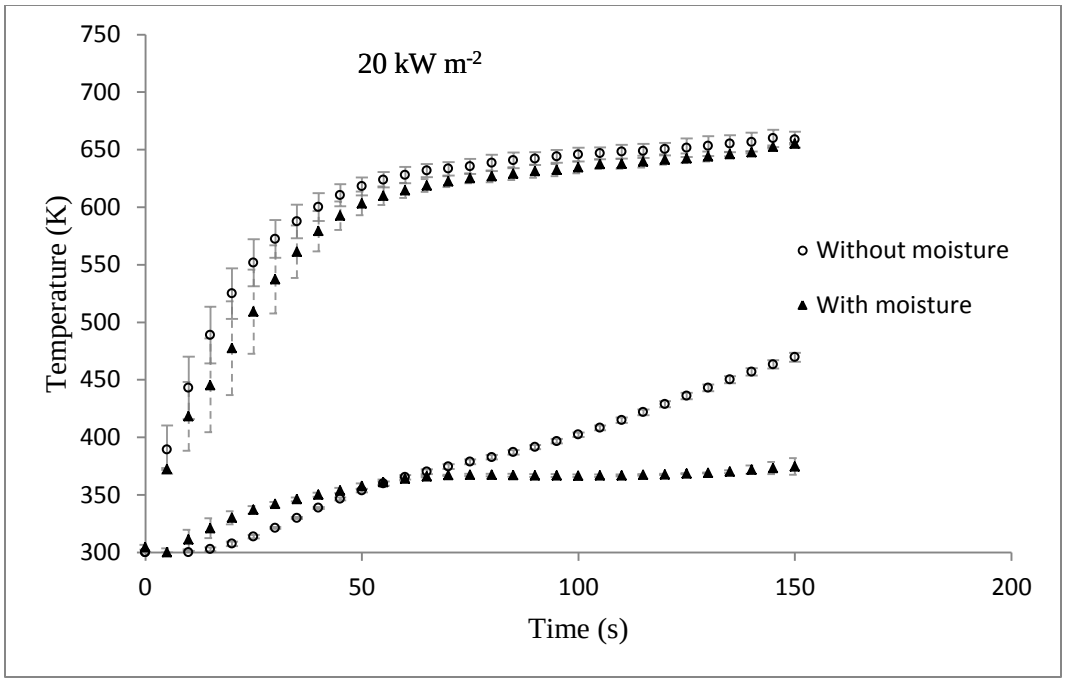
20 kW m-2
Temperature (K)
Time (s)
Without moisture
With moisture
750
700
650
600
550
500
450
400
350
300
0
50
100
150
200

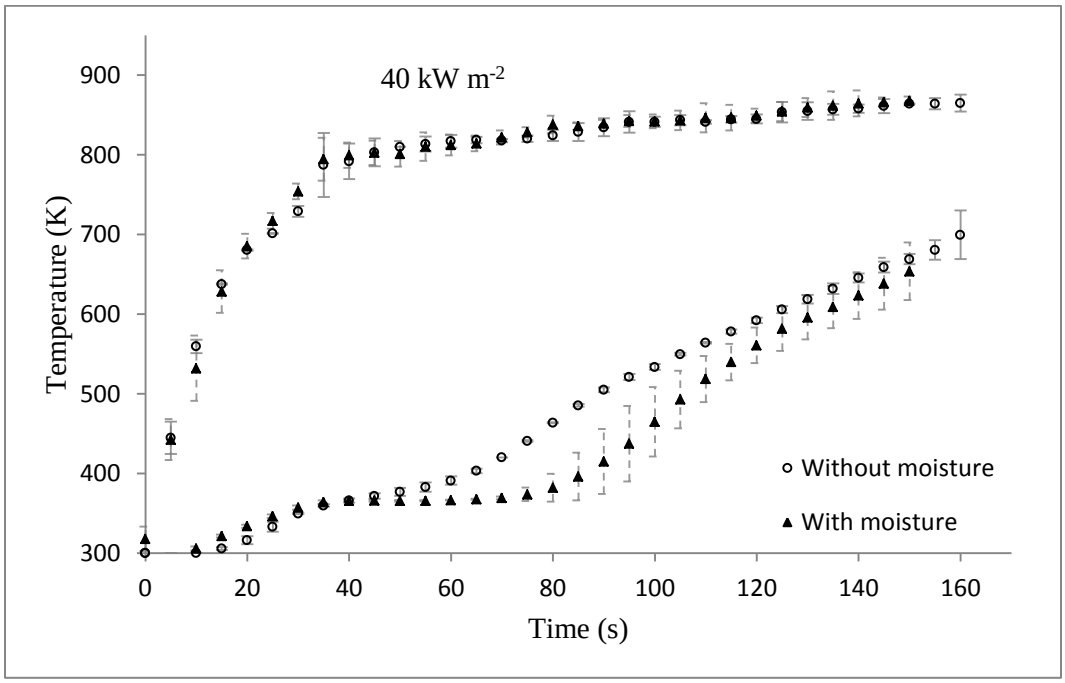
40 kW m-2
Temperature (K)
Time (s)
Without moisture
With moisture
900
800
700
600
500
400
300
0
20
40
60
80
100
120
140
160

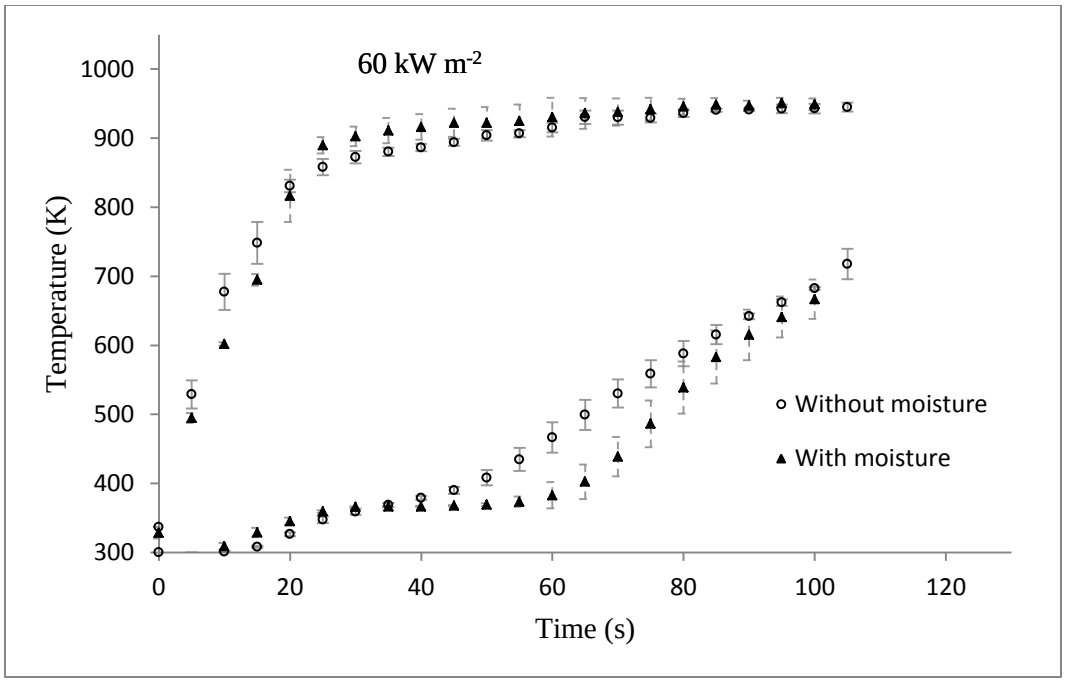

Figure 19. A comparison of the temperature profiles of samples with (12.6% water) and without added moisture (2% water) under anaerobic conditions.

A comparison of the mass loss profiles of samples with and without moisture is shown in Figure 20. The mass loss rate curves of the moisturized samples all have a sharp peak that occurred almost immediately after the test was started, representing the evaporation of the majority of the water in the sample. An examination of the temperature data confirmed that this peak occurred at close to 373 K, the boiling temperature of water. The mass loss rate profiles for the samples containing moisture generally had higher peaks and longer burn times. This is due to the mass added by the moisture.

Another way to compare the burning behavior of the moisturized and dry samples is through the final char yield. In the introduction section, it was noted that several researchers had found in other cellulosic materials that increasing the moisture content decreased the final char yields. This was found to be true for cardboard as well. The

moisturized samples had, on average, char yields 15% less than the char yields of the dry samples.

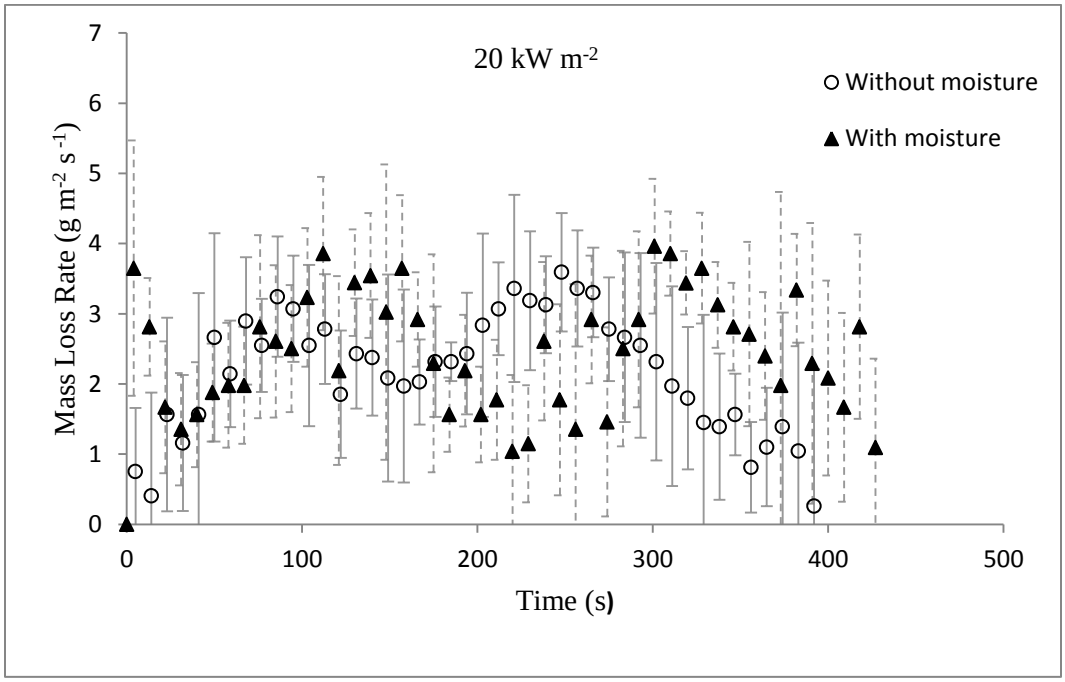

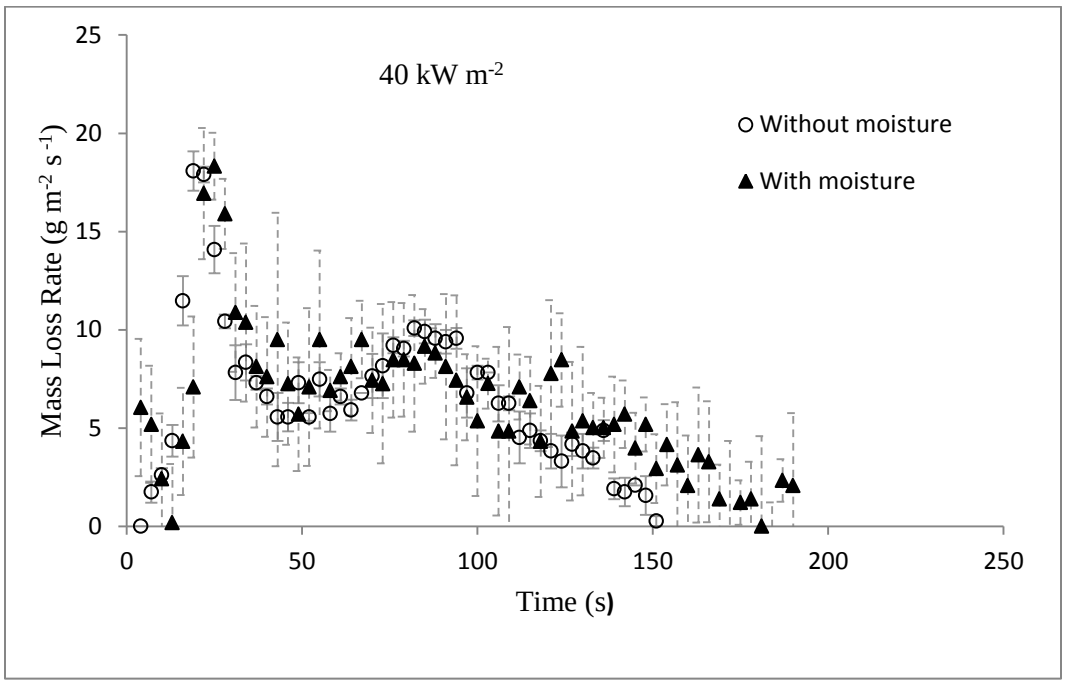

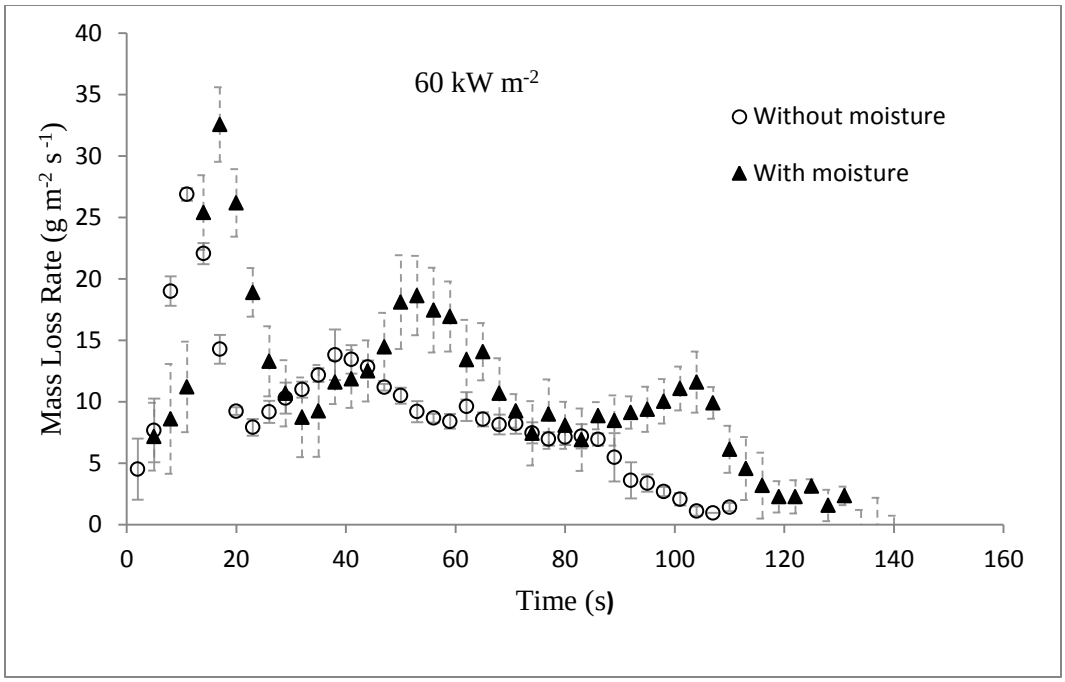

Figure 20. A comparison of the mass loss rate profiles of samples with and without added moisture under non-oxidative conditions.

4.3.1 Kinetics of Moisture and Model Development

In order to modify the existing anaerobic model to capture the effects of increased moisture, it was first necessary to understand the difference between the types of moisture present in the sample. In the original tests, the cardboard samples were dried using a desiccator before testing. From previous TGA tests it was observed that after the drying process, 2% moisture still remained in the sample. This moisture was different from the moisture that was added during the conditioning process. The 2% moisture was bound in the sample and fused with the sample particles. The 12.6 % moisture that was added during the conditioning process was not infused with the sample particles and sat in the holes or crevices within the sample. Therefore it evaporated much more easily. This evaporation produced the extremely sharp initial peak in the mass loss rate profiles.

In order to capture the evaporation of this less engrained moisture, it was necessary to change the kinetics of the evaporation reaction in the ThermaKin model. The original anaerobic model with just the moisture content modified and the evaporation kinetics left unchanged are shown in Figure 21.

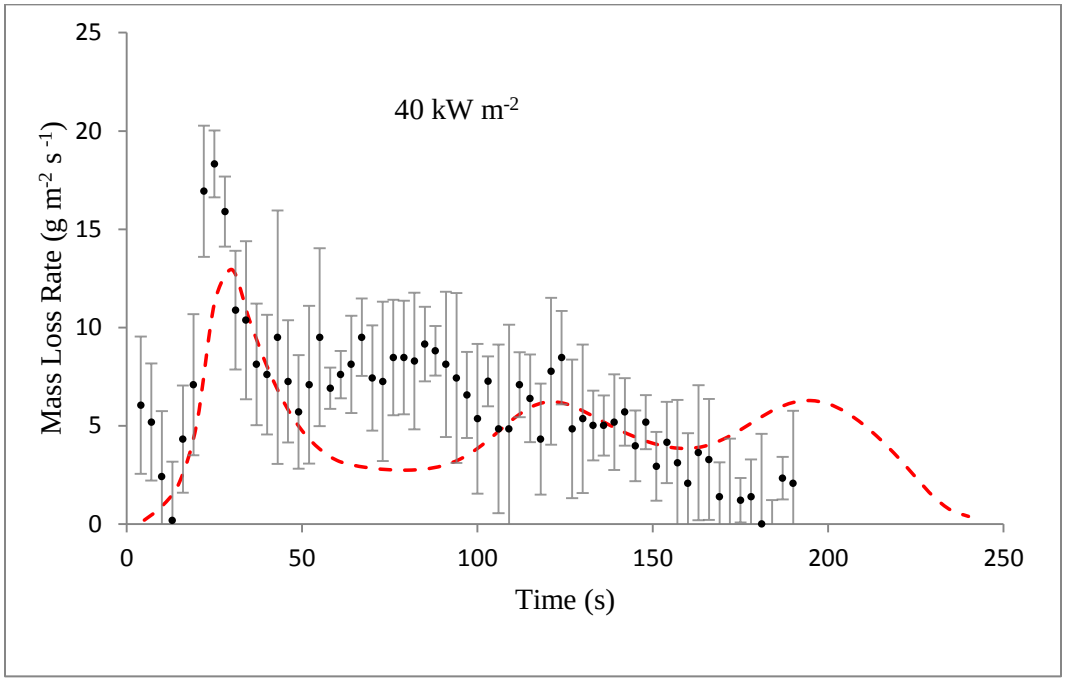

Figure 21. The mass loss rate profile with the ThermaKin model without the modified water evaporation reaction to reflect the evaporation of the added moisture content. It is clear that this model does not capture the initial evaporation spike as seen in Figure 10.

It is clear that this model does not capture the sharp evaporation peak at all. The kinetics of the evaporation reaction were meant to simulate the engrained moisture, not the moisture in the conditioned samples that was easy to evaporate. In order to capture the evaporation, the pre-exponential factor was set to one, and the activation energy was set to zero. This produced the following equation for the reaction rate constant:

$$k=Ae^{-Ea/(RT)}$$

$$k=1\ s^{-1}$$

This reaction had the effect of speeding up the rate of evaporation and making the reaction nearly instantaneous. Setting the activation energy equal to zero eliminated the time and temperature dependence of the reactions. ThermaKin allows the user to set a temperature at which the reaction starts. In this case, the activation temperature was set to 100 ºC. This has the effect of making the reaction controlled by heat transfer and not the kinetics of the model. In reality, the peak was much sharper than could be recreated by the model. To demonstrate this, the pre-exponential factor was varied to show that the resulting ThermaKin model did not visibly change. This is shown in Figure 22.

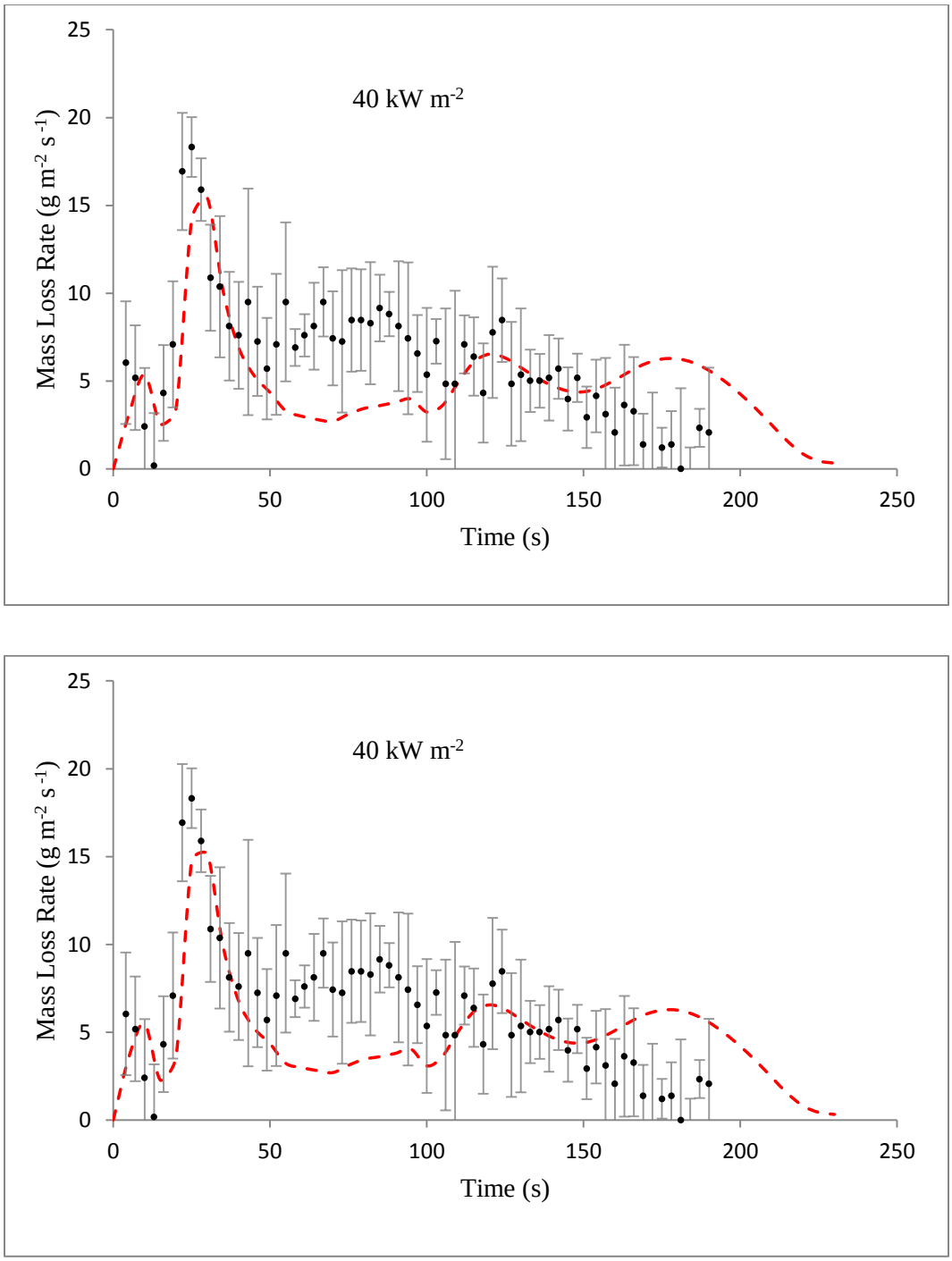

Figure 22. The mass loss rate profile of moisture conditioned samples at 40 kW m-2 with a ThermaKin model. The top figure shows the model with A=.5, E=0 and the bottom figure shows the model with A=2, E=0.

4.3.2 Results

The temperature data with the ThermaKin model is shown in Figure 23, with the evaporation reaction in the anaerobic model changed so the pre-exponential factor is one, and the activation energy is zero, as discussed above. The temperature of the top and bottom linerboards was generally under-predicted by the model. At 20 kW m^{-2} the top linerboard was over-predicted by .9% and the bottom was under-predicted by 1.7%. For 40 kW m^{-2} the top linerboard was under-predicted by 3.8% and the bottom linerboard by 7.9%. At 60 kW m^{-2} the top linerboard was under-predicted by 2.7% and the bottom by 6.9%. The error in the model was consistent with the error in the anaerobic model from the previous section; however, the anaerobic model generally over-predicted the experimental data, while the moisture model was generally under-predictive. Another way to view the error in the model is by the total average instantaneous difference for both the top and bottom linerboards. This gives an overall picture of the fit of the model and is a good way to compare to the anaerobic model. The instantaneous difference was 2.7%, 6%, and 6.2% for 20, 40, and 60 kW m^{-2} respectively. This was very similar to the error seen with the anaerobic temperature model.

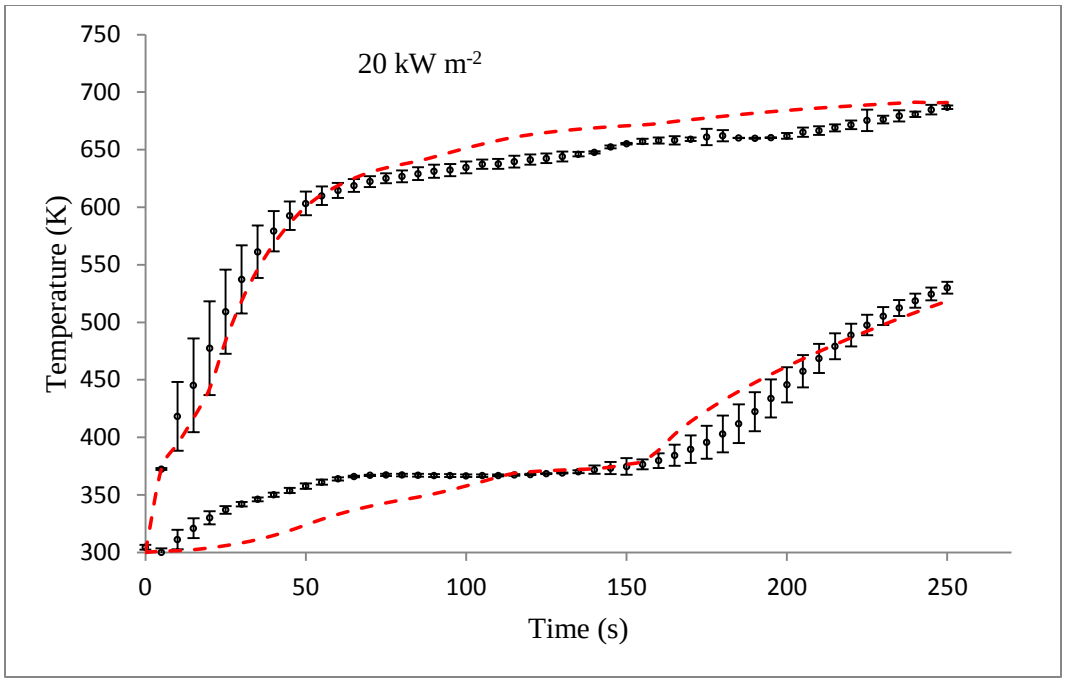
20 kW m-2
Temperature (K)
750
700
650
600
550
500
450
400
350
300
0
50
100
150
200
250
Time (s)

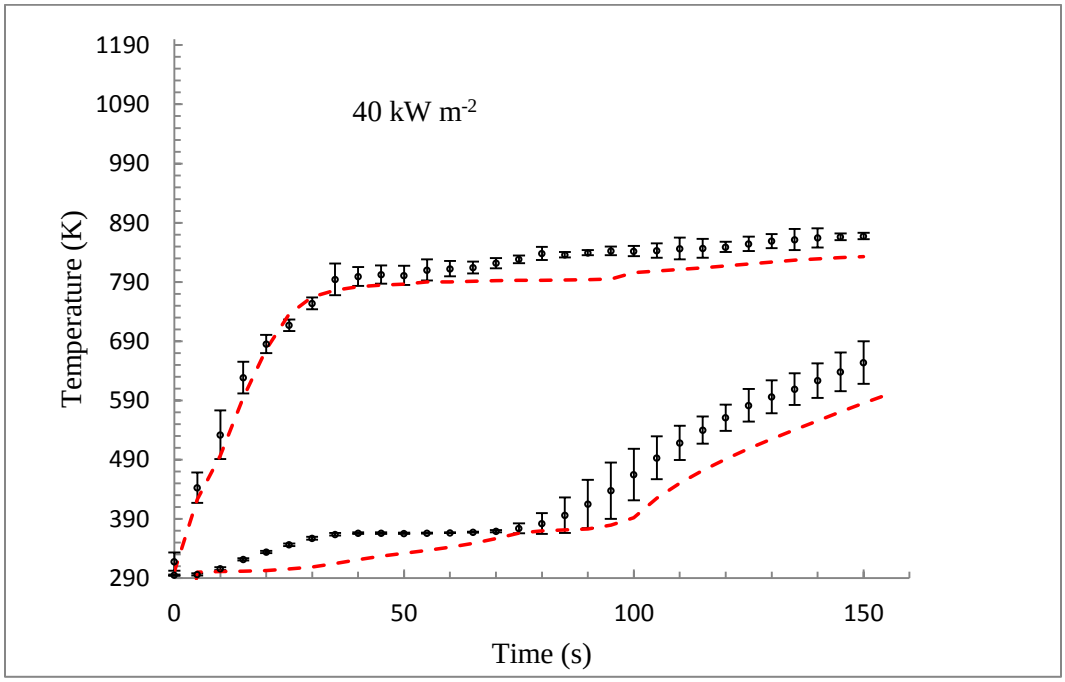
40 kW m-2
Temperature (K)
1190
1090
990
890
790
690
590
490
390
290
0
50
100
150
Time (s)

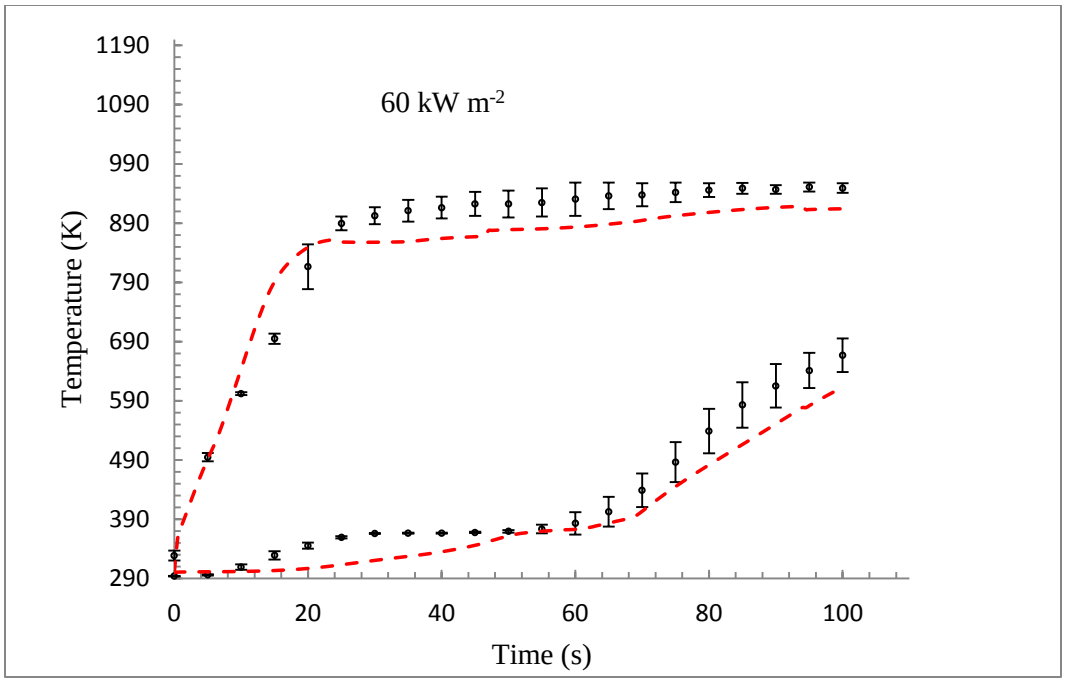

Figure 23. The temperature profiles for samples with added moisture with the ThermaKin model.

The mass loss rate profiles are shown in Figure 24. As with the temperature data set, the error in the model is comparable to the anaerobic model, not taking into account the initial mass loss rate spike attributed to evaporation. The initial moisture evaporation spike in the mass loss rate profile did not line up well with the peak produced by the model in magnitude or timing. The experimental peak was much larger than the one produced by the model, although the margin of error was quite large due to the extremely sharp nature of the peak. The experimental peak was also almost instantaneous, while the model peak took a few seconds to develop. One possible reason for the failure of the model to predict the evaporation peak is that, in the model, it was assumed that the measured moisture content was distributed evenly throughout the samples layers. In reality, this is not the case. After separating the layers of the cardboard after the conditioning period, it was clear that the outside linerboards contained slightly more

moisture than the inner linerboard. It was not possible to determine the exact moisture content of each specific layer due to the fact that the time it took to carefully separate the layers allowed for much of the moisture in the layers to evaporate, however it is clear that the moisture was not completely evenly distributed. This could have contributed to the very sharp and high nature of the evaporation peak as there is more moisture in the top layer to evaporate immediately.

Consistent with the anaerobic model, the first peak, after the initial evaporation peak, was predicted well. In the 20 kW m^{-2} model, the peak had a dip in the center, creating two peaks side by side within the larger initial peak. The maximum value was 2.95 g m^{-2} s^{-1}, compared to the experimental peak of 3.5 g m^{-2} s^{-1}. The maximum value in the model occurred at 125 seconds, and the experimental peak occurred at 130 seconds. The model for the 40 and 60 kW m^{-2} data did not have the dual initial peaks. The timing and height of the initial peaks in these tests agreed well with the model. The agreement increased as the heat flux increased. The first peak was under-predicted by 15.7, 16.4, and 6.1% for 20, 40, and 60 20 kW m^{-2}. The timing of the peak was early by 10 seconds and 3 second for 20 and 40 kW m^{-2} respectively, and late for the 40 kW m^{-2} data by 5 seconds.

The model did not predict total burning time well for the 20 and 40 kW m^{-2} data. The 20 kW m^{-2} data was over-predicted by over 350 seconds, the 40 kW m^{-2} data by 40 seconds, and the 60 kW m^{-2} data was almost exactly predicted by the model. This was the exact same trend followed by the anaerobic section.

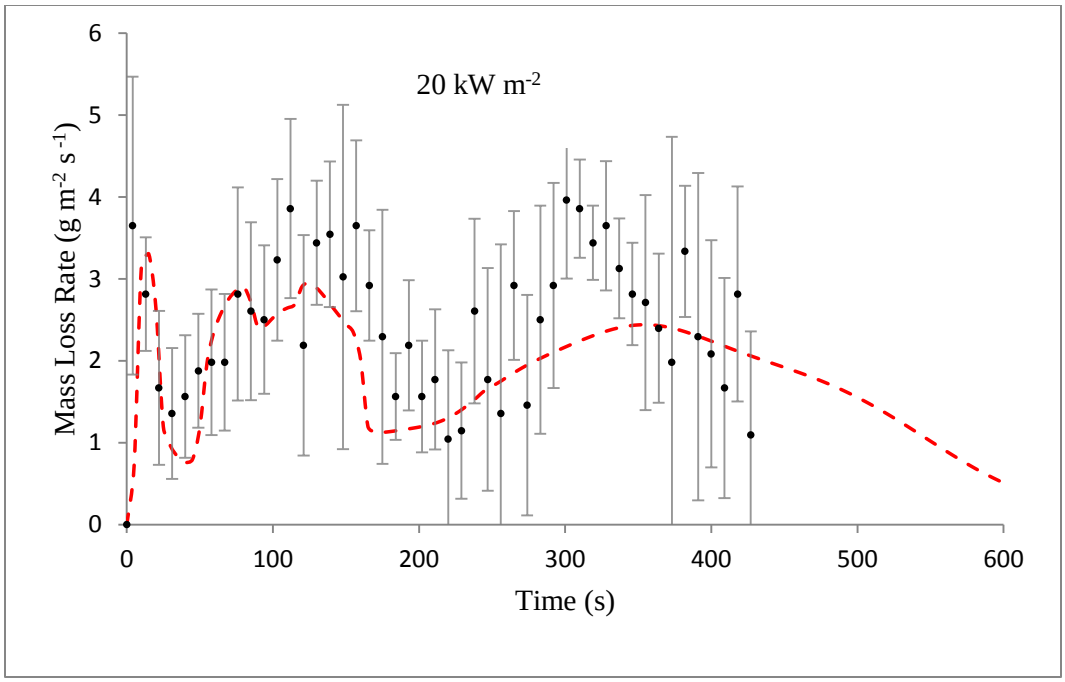
20 kW m-2
Mass Loss Rate (g m-2 s-1)
Time (s)
0
1
2
3
4
5
6
0
100
200
300
400
500
600

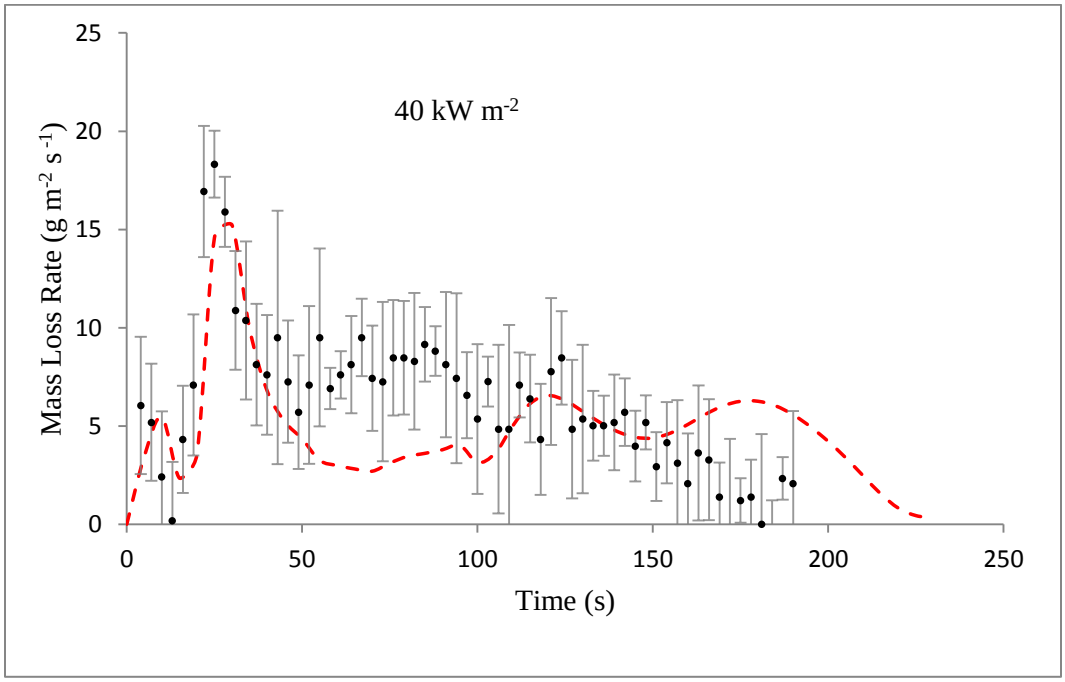
40 kW m-2
Mass Loss Rate (g m-2 s-1)
Time (s)
0
5
10
15
20
25
0
50
100
150
200
250

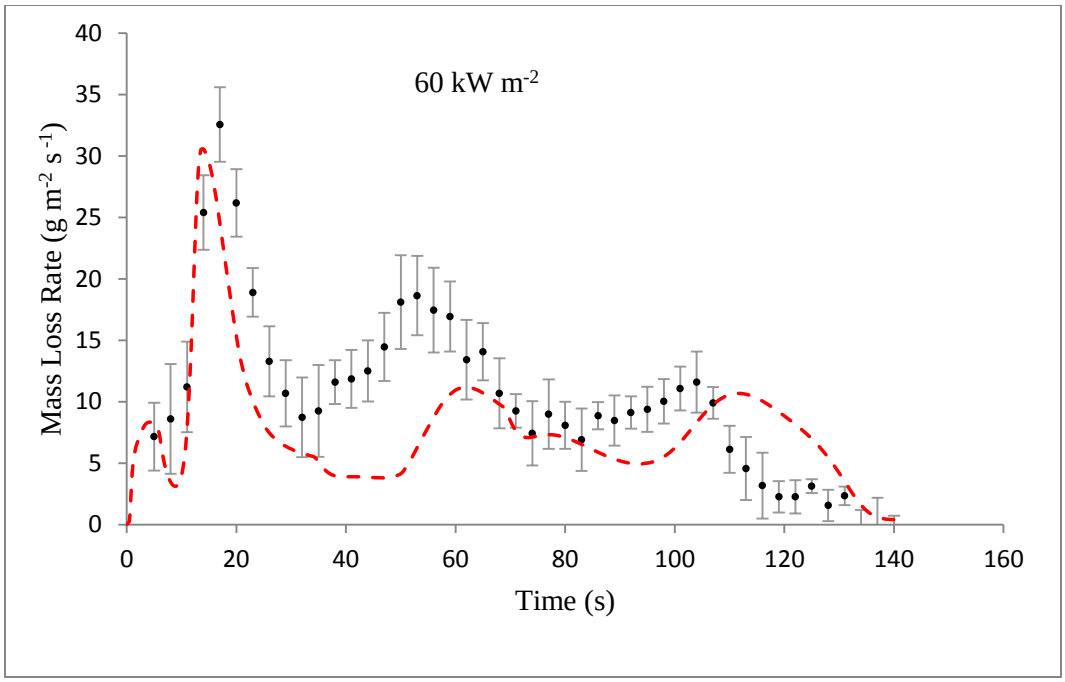

Figure 24. The mass loss rate profiles for the samples with added moisture with the ThermaKin Model.

The moisture model was adapted to the anaerobic model to examine if the modification of the evaporation reaction could improve the fit of the model. When the moisture in the sample was adjusted back to 2%, but the evaporation mechanism was left in the modified version, the instantaneous error in the temperature increased. The mass loss rate profiles at 20 and 40 kW m^{-2} were marginally improved, primarily because the faster evaporation reaction slightly increased the first peak, but since the fit of the temperature profile was the designated criteria for the model, the modified moisture reaction was not adapted into the anaerobic model. This supports the claim made earlier in this section, that the moisture held in the sample naturally reacts differently than moisture added to the sample.

5. CONCLUSIONS

A new device termed the Controlled Atmosphere Pyrolysis Apparatus (or CAPA) was developed in order to perform gasification tests in a standard cone calorimeter. This apparatus can be manually placed underneath the cone heater and, given a single, or a combination of gases, the atmosphere above the sample can be set. This apparatus represents a significant advancement in gasification testing because it allows a user to perform these tests without the need for a designated piece of equipment. The CAPA is safe and easy to use.

Gasification tests were conducted in the CAPA using double-walled corrugated cardboard at 2.2 and 10.5 vol.% oxygen. The conditions chosen represent the lowest attainable concentration of oxygen and the highest concentration at which the sample does not ignite. These atmospheres are meant to represent non-oxidative or anaerobic pyrolysis and oxidative pyrolysis without the presence of a flame. Temperature and mass loss rate profiles were collected separately for each atmospheric condition at 20, 40, and 60 kW m^{-2}. The temperature profiles were used to fit the model and the mass loss rate profiles were used as validation of the model.

A one-dimensional pyrolysis model called ThermaKin was used to create a universal model for the pyrolysis of the corrugated cardboard. Previous work was done on the development of the model under flaming conditions. This work was continued and presented in this thesis. It was found that for the non-oxidative pyrolysis tests presented in this thesis, the previously developed model provided the best fit of the data. The model was able to predict the mass loss rate profiles to within 13% across all heat fluxes.

This model was then adapted to predict oxidative pyrolysis of the corrugated cardboard. In order to do this, four oxidation reactions were fit to TGA data collected at 10% and 21% oxygen. These new reactions, along with the four non-oxidative reactions that comprised the anaerobic model formed the oxidative model. The four added reaction work to oxidize the chars and convert them to ash. This model was able to predict the mass loss rate profiles to within 18% across all the heat fluxes.

The effects of moisture were examined as well by adding water vapor to the samples through uniform conditioning. . The moisture model was adapted by making the kinetics of the evaporation reaction much faster to reflect the rapid evaporation of water observed in the mass loss rate experiments. The moisture model was able to predict the mass loss rate profiles across all the heat fluxes to within 20%.

The ThermaKin model is able to capture the essential burning behavior corrugated cardboard samples. The samples exhibit behavior which cannot be compensated for in the model, like shrinking, peeling, and exfoliation, and therefore it was not realistic that all of the peaks and valleys of the mass loss rate profiles would be captured. The error between the model and experimental data is quite consistent between the non-oxidative, oxidative, and moisturized gasification conditions, indicating that the model succeeds in modeling all the conditions examined.

APPENDIX A-ThermaKin Input Files

The input files for the ThermaKin simulations are shown below. There are two files necessary to run a simulation: a component file and a condition file. The component file establishes the thermophysical properties of each of the components being utilized and allows the user to designate the reaction scheme. The conditions file contains the structure of the sample, created from the various components listed in the components file, as well as the top and bottom boundary conditions and the integration parameters. The component file is the same for all simulations, while the condition files changes based on the atmosphere. The exception to this is the moisture model, where the evaporation reaction is modified in the component file. The components used in this project are defined in the table below. The numbers 1-3 indicated which layer of the sample is being described. 1 corresponds to the linerboard, 2 corresponds to the C-flute layer, and 3 corresponds to the B-flute layer. For example, CB_B1 would be the virgin linerboard material.

ThermaKin component	**Definition**
CB_A	Moisture
CB_B(1-3)	The virgin corrugated cardboard
CB_C(1-3)	The intermediary, defined as a halfway point between the virgin material and the first char
CB_ch(1-3)	The initial char
CB_ch(4-6)	The final char
CB_g_1	Moisture vapor
CB_g_2	Volatiles

Cardboard.cmp-Component file

```
COMPONENT:       O2
STATE:           G
DENSITY:         10000  0  0  0
HEAT CAPACITY:   827  .35  -8.9e-5  2
CONDUCTIVITY:    0.1  0  0  0
TRANSPORT:       1e-5  0  0 0
EMISSIVITY & ABSORPTION:  0.7  1000

COMPONENT:       CB_A
STATE:           S
DENSITY:         10000  0  0  0
HEAT CAPACITY:   5230  -6.71  0.011  2
CONDUCTIVITY:    0.1  0  0  0
TRANSPORT:       1e-5  0  0 0
EMISSIVITY & ABSORPTION:  0.7  1000

COMPONENT:       CB_B1
STATE:           S
DENSITY:         520  0  0  0
HEAT CAPACITY:   1800  0  0  0
CONDUCTIVITY:    0.1  0  0  0
TRANSPORT:       1e-5  0  0 0
EMISSIVITY & ABSORPTION:  0.7  1000

COMPONENT:       CB_B2
STATE:           S
DENSITY:         49  0  0  0
HEAT CAPACITY:   1800  0  0  0
CONDUCTIVITY:    0.1  0  0  0
TRANSPORT:       1e-5  0  0 0
EMISSIVITY & ABSORPTION:  0.7  1000

COMPONENT:       CB_B3
STATE:           S
DENSITY:         74  0  0  0
HEAT CAPACITY:   1800  0  0  0
CONDUCTIVITY:    0.1  0  0  0
TRANSPORT:       1e-5  0  0 0
EMISSIVITY & ABSORPTION:  0.7  1000

COMPONENT:       CB_C1
STATE:           S
DENSITY:         468  0  0  0
HEAT CAPACITY:   1540  0  0  0
CONDUCTIVITY:    0.05  0  7.5e-11  3
TRANSPORT:       1e-5  0  0 0
EMISSIVITY & ABSORPTION:  0.775  1000

COMPONENT:       CB_C2
STATE:           S
DENSITY:         44  0  0  0
HEAT CAPACITY:   1540  0  0  0
```

```
CONDUCTIVITY:    0.05  0  7.5e-10  3
TRANSPORT:       1e-5  0  0 0
EMISSIVITY & ABSORPTION:  0.775  1000

COMPONENT:       CB_C3
STATE:           S
DENSITY:         67  0  0  0
HEAT CAPACITY:   1540  0  0  0
CONDUCTIVITY:    0.05 0 7.5e-10  3
TRANSPORT:       1e-5  0  0 0
EMISSIVITY & ABSORPTION:  0.775  1000

COMPONENT:       CB_ch1
STATE:           S
DENSITY:         173  0  0  0
HEAT CAPACITY:   1280  0  0  0
CONDUCTIVITY:    0  0  1.5e-10  3
TRANSPORT:       1e-5  0  0 0
EMISSIVITY & ABSORPTION:  .85  1000

COMPONENT:       CB_ch2
STATE:           S
DENSITY:         16  0  0  0
HEAT CAPACITY:   1280  0  0  0
CONDUCTIVITY:    0  0  1.5e-9  3
TRANSPORT:       1e-5  0  0 0
EMISSIVITY & ABSORPTION:  .85 1000

COMPONENT:       CB_ch3
STATE:           S
DENSITY:         25  0  0  0
HEAT CAPACITY:   1280  0  0  0
CONDUCTIVITY:    0  0  1.5e-9  3
TRANSPORT:       1e-5  0  0 0
EMISSIVITY & ABSORPTION:  .85  1000

COMPONENT:       CB_ch4
STATE:           S
DENSITY:         102  0  0  0
HEAT CAPACITY:   1280  0  0  0
CONDUCTIVITY:    0  0 1.5e-10  3
TRANSPORT:       1e-5  0  0 0
EMISSIVITY & ABSORPTION:  .85 1000

COMPONENT:       CB_ch5
STATE:           S
DENSITY:         9.4  0  0  0
HEAT CAPACITY:   1280  0  0  0
CONDUCTIVITY:    0  0  1.5e-9  3
TRANSPORT:       1e-5  0  0 0
EMISSIVITY & ABSORPTION:  .85  1000
COMPONENT:       CB_ch6

STATE:           S
DENSITY:         14.8  0  0  0
```

```
HEAT CAPACITY:   1280  0  0  0
CONDUCTIVITY:    0  0  1.5e-9  3
TRANSPORT:       1e-5  0  0 0
EMISSIVITY & ABSORPTION:  .85 1000

COMPONENT:       CB_g_1
STATE:           G
DENSITY:         10000  0  0  0
HEAT CAPACITY:   2398  -1.6  0.0016  2
CONDUCTIVITY:    0.1  0  0  0
TRANSPORT:       1e-5  0  0 0
EMISSIVITY & ABSORPTION:  0.7  1000

COMPONENT:       CB_g_2
STATE:           G
DENSITY:         10000  0  0  0
HEAT CAPACITY:   1280  0  0  0
CONDUCTIVITY:    0.1  0  0  0
TRANSPORT:       1e-5  0  0 0
EMISSIVITY & ABSORPTION:  0.7  1000

COMPONENT:      KAOWOOL
STATE:          S
DENSITY:        256  0  0  0
HEAT CAPACITY:  1070  0  0  0
CONDUCTIVITY:   0.0519  -4e-5  1e-7  2
TRANSPORT:      1e-30  0  0  0
EMISSIVITY & ABSORPTION:  0  1000

COMPONENT:      ASH1
STATE:          S
DENSITY:        15.3 0  0  0
HEAT CAPACITY:  1280  0  0  0
CONDUCTIVITY:   0  0  .15e-9  3
TRANSPORT:      1e-5  0  0 0
EMISSIVITY & ABSORPTION:  .85  1000

COMPONENT:      ASH2
STATE:          S
DENSITY:        1.41 0  0  0
HEAT CAPACITY:  1280  0  0  0
CONDUCTIVITY:   0  0  1.5e-9  3
TRANSPORT:      1e-5  0  0 0
EMISSIVITY & ABSORPTION:  .85  1000

COMPONENT:      ASH3
STATE:          S
DENSITY:        2.22 0  0  0
HEAT CAPACITY:  1280  0  0  0
CONDUCTIVITY:   0  0  1.5e-9  3
TRANSPORT:      1e-5  0  0 0
EMISSIVITY & ABSORPTION:  .85  1000

MIXTURES
S SWELLING:           0
```

```
L SWELLING:           0
G SWELLING LIMIT:     1e-30
PARALL CONDUCTIVITY:  0.5
PARALL TRANSPORT:     0.5

REACTION:       CB_A + NOCOMP -> NOCOMP + CB_g_1
STOICHIOMETRY:  1      0         0        1
ARRHENIUS:      6.14e0  2.35e4
HEAT:           -24.45e5  0  0  0
TEMP LIMIT:     L  300

REACTION:       CB_B1 + NOCOMP -> CB_C1 + CB_g_2
STOICHIOMETRY:  1      0         0.9     0.1
ARRHENIUS:      7.95e9  1.3e5
HEAT:           0  0  0  0
TEMP LIMIT:     L  300

REACTION:       CB_B2 + NOCOMP -> CB_C2 + CB_g_2
STOICHIOMETRY:  1      0         0.9     0.1
ARRHENIUS:      7.95e9  1.3e5
HEAT:           0  0  0  0
TEMP LIMIT:     L  300

REACTION:       CB_B3 + NOCOMP -> CB_C3 + CB_g_2
STOICHIOMETRY:  1      0         0.9     0.1
ARRHENIUS:      7.95e9  1.3e5
HEAT:           0  0  0  0
TEMP LIMIT:     L  300

REACTION:       CB_C1 + NOCOMP -> CB_ch1 + CB_g_2
STOICHIOMETRY:  1      0         0.37     0.63
ARRHENIUS:      2e11  1.6e5
HEAT:           -1.26e5  0  0  0
TEMP LIMIT:     L  300

REACTION:       CB_C2 + NOCOMP -> CB_ch2 + CB_g_2
STOICHIOMETRY:  1      0         0.37     0.63
ARRHENIUS:      2e11  1.6e5
HEAT:           -1.26e5  0  0  0
TEMP LIMIT:     L  300

REACTION:       CB_C3 + NOCOMP -> CB_ch3 + CB_g_2
STOICHIOMETRY:  1      0         0.37     0.63
ARRHENIUS:      2e11  1.6e5
HEAT:           -1.26e5  0  0  0
TEMP LIMIT:     L  300

REACTION:       CB_C1 + O2 -> CB_ch1 + CB_g_2
STOICHIOMETRY:  1      0         0.59     .41
ARRHENIUS:      75.22e10  1.6e5
HEAT:           0  0  0  0
TEMP LIMIT:     L  300

REACTION:       CB_C2 + O2 -> CB_ch2 + CB_g_2
STOICHIOMETRY:  1      0         0.59     .41
```

```
ARRHENIUS:      75.22e10  1.6e5
HEAT:           0  0  0  0
TEMP LIMIT:     L  300

REACTION:       CB_C3 + O2 -> CB_ch3 + CB_g_2
STOICHIOMETRY:  1      0         0.59     .41
ARRHENIUS:      75.22e10  1.6e5
HEAT:           0  0  0  0
TEMP LIMIT:     L  300

REACTION:       CB_C1 + O2 -> CB_ch1 + CB_g_2
STOICHIOMETRY:  1      0         0.48     0.52
ARRHENIUS:      17.22e22  2.8e5
HEAT:           0  0  0  0
TEMP LIMIT:     L  300

REACTION:       CB_C2 + O2 -> CB_ch2 + CB_g_2
STOICHIOMETRY:  1      0         0.48     0.52
ARRHENIUS:      17.22e22  2.8e5
HEAT:           0  0  0  0
TEMP LIMIT:     L  300

REACTION:       CB_C3 + O2 -> CB_ch3 + CB_g_2
STOICHIOMETRY:  1      0         0.48     0.52
ARRHENIUS:      17.22e22  2.8e5
HEAT:           0  0  0  0
TEMP LIMIT:     L  300

REACTION:       CB_ch1 + NOCOMP -> CB_ch4 + CB_g_2
STOICHIOMETRY:  1      0         0.59     0.41
ARRHENIUS:      2.61e-2  1.7e4
HEAT:           0  0  0  0
TEMP LIMIT:     L  300

REACTION:       CB_ch2 + NOCOMP -> CB_ch5 + CB_g_2
STOICHIOMETRY:  1      0         0.59     0.41
ARRHENIUS:      2.61e-2  1.7e4
HEAT:           0  0  0  0
TEMP LIMIT:     L  300

REACTION:       CB_ch3 + NOCOMP -> CB_ch6 + CB_g_2
STOICHIOMETRY:  1      0         0.59     0.41
ARRHENIUS:      2.61e-2  1.7e4
HEAT:           0  0  0  0
TEMP LIMIT:     L  300

REACTION:       CB_ch1 + O2 -> CB_ch4 + CB_g_2
STOICHIOMETRY:  1      .95       0.48     1.47
ARRHENIUS:      17.9e-2  1.7e4
HEAT:           1.25e7  0  0  0
TEMP LIMIT:     L  300

REACTION:       CB_ch2 + O2 -> CB_ch5 + CB_g_2
STOICHIOMETRY:  1      .95       0.48     1.47
ARRHENIUS:      17.9e-2  1.7e4
```

```
HEAT:           1.25e7  0  0  0
TEMP LIMIT:     L  300

REACTION:       CB_ch3 + O2 -> CB_ch6 + CB_g_2
STOICHIOMETRY:  1      .95       0.48     1.47
ARRHENIUS:      17.9e-2  1.7e4
HEAT:           1.25e7  0  0  0
TEMP LIMIT:     L  300

REACTION:       CB_ch4 + O2 -> ASH1 + CB_g_2
STOICHIOMETRY:  1      1.56       0.15     2.4
ARRHENIUS:      1.16416e80  1.084e6
HEAT:           2.04e7  0  0  0
TEMP LIMIT:     L  300

REACTION:       CB_ch5 + O2 -> ASH2 + CB_g_2
STOICHIOMETRY:  1      1.56       0.15     2.4
ARRHENIUS:      1.16416e80  1.084e6
HEAT:           2.04e7  0  0  0
TEMP LIMIT:     L  300

REACTION:       CB_ch6 + O2 -> ASH3 + CB_g_2
STOICHIOMETRY:  1      1.56       0.15     2.4
ARRHENIUS:      1.16416e80  1.084e6
HEAT:           2.04e7  0  0  0
TEMP LIMIT:     L  300
```

The condition files changes based on the gas atmosphere the sample is gasified in. The files below all show a heat flux of 20 kW m^{-2}.

Cardboard_Pyrolysis_no02.cnd
Non-Oxidative Pyrolysis

```
OBJECT TYPE:  1D

OBJECT STRUCTURE
****************

THICKNESS:  0.00064
TEMPERATURE:  300
MASS FRACTIONS:
CB_B1  0.98
CB_A   0.02

THICKNESS:  0.0034
TEMPERATURE:  300
MASS FRACTIONS:
CB_B2  0.98
CB_A   0.02

THICKNESS:  0.00064
```

```
TEMPERATURE:  300
MASS FRACTIONS:
CB_B1  0.98
CB_A   0.02

THICKNESS:  0.0021
TEMPERATURE:  300
MASS FRACTIONS:
CB_B3  0.98
CB_A   0.02

THICKNESS:  0.00064
TEMPERATURE:  300
MASS FRACTIONS:
CB_B1  0.98
CB_A   0.02

THICKNESS:  0.028
TEMPERATURE:  305
MASS FRACTIONS:
KAOWOOL  1

OBJECT BOUNDARIES
*****************

TOP BOUNDARY

MASS TRANSPORT: YES
CB_g_1  LIN  0.05  0
CB_g_2  LIN  0.05  0

OUTSIDE TEMP TIME PROG: 330  0
CONVECTION COEFF:  5

EXTERNAL RADIATION: YES
TIME PROG1: 2.0e4  0  6.0e2
TIME PROG2:  0  0 0

REPEAT:  NO
ABSORPTION MODE: MAX

FLAME: NO


BOTTOM BOUNDARY

MASS TRANSPORT:  NO

OUTSIDE TEMP TIME PROG:  300  0
CONVECTION COEFF:  0

EXTERNAL RADIATION:  NO

FLAME:  NO
```

INTEGRATION PARAMETERS
****

ELEMENT SIZE: 5e-5
TIME STEP: 0.05
DURATION: 600

OUTPUT FREQUENCY:
ELEMENTS: 1
TIME STEPS: 100

Cardboard_pyrolysis_with02.cnd
Oxidative Pyrolysis

OBJECT TYPE: 1D

OBJECT STRUCTURE
****

THICKNESS: 0.00064
TEMPERATURE: 300
MASS FRACTIONS:
CB_B1 0.98
CB_A   0.02

THICKNESS: 0.0034
TEMPERATURE: 300
MASS FRACTIONS:
CB_B2 0.98
CB_A   0.02

THICKNESS: 0.00064
TEMPERATURE: 300
MASS FRACTIONS:
CB_B1 0.98
CB_A   0.02

THICKNESS: 0.0021
TEMPERATURE: 300
MASS FRACTIONS:
CB_B3 0.98
CB_A   0.02

THICKNESS: 0.00064
TEMPERATURE: 300
MASS FRACTIONS:
CB_B1 0.98
CB_A   0.02

THICKNESS: 0.028
TEMPERATURE: 305
MASS FRACTIONS:
KAOWOOL 1

```
OBJECT BOUNDARIES
*****************

TOP BOUNDARY

MASS TRANSPORT: YES
CB_g_1  LIN  0.05  0
CB_g_2  LIN  0.05  0
O2      LIN  0.05  .0000067

OUTSIDE TEMP TIME PROG: 330  0
CONVECTION COEFF:  5

EXTERNAL RADIATION: YES
TIME PROG1:  2.0e4  0  3.5e2
TIME PROG2:  0  0 0

REPEAT:  NO
ABSORPTION MODE: MAX

FLAME: NO


BOTTOM BOUNDARY

MASS TRANSPORT:  NO

OUTSIDE TEMP TIME PROG:  300  0
CONVECTION COEFF:  0

EXTERNAL RADIATION:  NO

FLAME:  NO

INTEGRATION PARAMETERS
**********************

ELEMENT SIZE:  5e-5
TIME STEP:     0.005
DURATION:      350

OUTPUT FREQUENCY:
ELEMENTS:    1
TIME STEPS:  1000
```

WORKS CITED

1. Marcos Chaos, Mohammed M. Khan, Sergey B. Dorofeev. *Pyrolysis of corrugated cardboard in inert and oxidative environments.* Proceedings of the Combustion Institute, Volume 34, Issue 2, 2013, Pages 2583-2590, ISSN 1540-7489, http://dx.doi.org/10.1016/j.proci.2012.06.031.

2. *Warehouse commodity classification from fundamental principles Part I: Commodity & burning rates.* Gollner, M. J., et al. 2011, Fire Safety Journal, pp. 305-316.

3. *Experiments and Modeling of Single- and Triple-Wall Corrugated Cardboard: Effective Material Properties and Fire Behavior*. Chaos, Marcos, et al. 2011, Fire and Materials, pp. 625-636.

4. *The Application of a Genetic Algorithm to Estimate Material Properties for Fire Modeling from Bench-Scale Fire Test Data*. Lautenberger, C., Rein, G. and Fernandez-Pello, C. 2006, Fire Safety Journal, pp. 204-214.

5. Liu, Xuan. *Design and Analysis of New Gasification Apparatus based on the Standard Cone Calorimeter* (Master's Thesis). 2012, University of Maryland, College Park.

6. Austin, P.J., R.R Buch, and T. Kashiwagi. *Gasification of Silicone Fluids under External Thermal Radiation*. NISTIR 6041, 1997.

7. Stoliarov, I. Stanislav, et al. *Prediction of the Burning Rates of Charring Polymers.* Atlantic City : Federal Aviation Administration, 2010. DOT/FAA/AR-TN09/59.

8. Stoliarov, Stanislav I., et al. Prediction of the burning rates of non-charring polymers. *Combustion and Flame.* 2009, Vol. 156.

9. Stoliarov, S. I. and Lyon, R. E. *Thermo-Kinetic Model of Burning.* Atlantic City : Federal Aviation Administration, 2008.

10. Pérez, S., Samain, D. *Structure and Engineering of Celluloses*, In: Derek Horton, Editor(s), Advances in Carbohydrate Chemistry and Biochemistry, Academic Press, 2010, Volume 64, Pages 25-116, http://dx.doi.org/10.1016/S0065-2318(10)64003-6.

11. David, C., et al. *Determination of a reaction scheme for cardboard thermal degradation using thermal gravimetric analysis*. *Journal of Analytical Applied Pyrolysis.* 2003, 67.

12. Witkowski, Artur. *The Use of Numerical Methods to Interpret Polymer Decomposition Data (*Doctoral thesis). 2012, University of Central Lancashire.

13. Ohlemiller, T.J. *Smoldering Combustion*. National Fire Protection Association, & Society of Fire Protection Engineers. 1995, *SFPE handbook of fire protection engineering, Chapter 11, pp. 2/171-179*. Quincy, Mass: National Fire Protection Association.

14. Gupta, Ashwani and Muller, Patric. *Pyrolysis of paper and Cardboard in Inert and Oxidative Environments*. *Journal of Propulsion and Power.* 1999, Vol. 15, 2.

15. T. Fateh, T. Rogaume, J. Luche, F. Richard, F. Jabouille, *Kinetic and mechanism of the thermal degradation of a plywood by using thermogravimetry and Fourier-transformed infrared spectroscopy analysis in nitrogen and air atmosphere*, Fire Safety Journal, Volume 58, May 2013, Pages 25-37, ISSN 0379-7112, http://dx.doi.org/10.1016/j.firesaf.2013.01.019.

16. McKinnon, Mark B., Stoliarov, Stanislav I. and Witkowski, Artur. *Development of a Pyrolysis Model for Corrugated Cardboard.* 2013, Combustion and Flame.

17. *Effects of External Radiant Heat Flux and Ambient Oxygen Concentration on nonlaming Gasification Rates and Evolved Products of White Pine.* Kashiwagi, T., Ohlemiller, T. J. and Werner, K. 1987, Combustion and Flame, pp. 331-345.

18. Chris Lautenberger, Carlos Fernandez-Pello. *A model for the oxidative pyrolysis of wood*. Combustion and Flame, Volume 156, Issue 8, August 2009, Pages 1503-1513, ISSN 0010-2180, http://dx.doi.org/10.1016/j.combustflame.2009.04.001.

19. Marcos Chaos, Mohammed M. Khan, Sergey B. Dorofeev, *Pyrolysis of corrugated cardboard in inert and oxidative environments*, Proceedings of the Combustion Institute, Volume 34, Issue 2, 2013, Pages 2583-2590, ISSN 1540-7489, http://dx.doi.org/10.1016/j.proci.2012.06.031.

20. Su, Yi, et al. *Effect of Moisture Content on Rice Straw Pyrolysis Behavior*. 2010, *Proceedings of the CSEE* 26: 019.

21. Yao Bin Yang, Anh N Phan, Changkook Ryu, Vida Sharifi, Jim Swithenbank, *Mathematical modelling of slow pyrolysis of segregated solid wastes in a packed-bed pyrolyser*, Fuel, Volume 86, Issues 1–2, January 2007, Pages 169-180, ISSN 0016-2361, http://dx.doi.org/10.1016/j.fuel.2006.07.012.

22. *Pyrolysis of a wood-derived material. Effects of moisture and ash content*. Murray R. Gray, William H. Corcoran, and George R. Gavalas. *Industrial & Engineering Chemistry Process Design and Development* 1985 *24* (3), 646-651, http://dx.doi.org /10.1021/i200030a020.

23. ASTM International. *Standard Test Method for Heat and Visible Smoke Release Rates for Materials and Products Using an Oxygen Consumption Calorimeter.* s.l. : ASTM, 2009. E 1354-09.

24. McKinnon, Mark. *Development of a Model for Flaming Combustion of Double-Wall Corrugated Cardboard* (Master's thesis). 2012, University of Maryland, College Park.